Reassessment of Middle Devonian dolomite, Presqu'ile barrier, Northwest Territories

M. Coniglio[1], D.W. Morrow[2], and N. Wilson[2*]

Coniglio, M., Morrow, D.W., and Wilson, N., 2006: Reassessment of Middle Devonian dolomite, Presqu'ile barrier, Northwest Territories; *in* Potential for Carbonate-hosted Lead-zinc Mississippi Valley-type Mineralization in Northern Alberta and Southern Northwest Territories: Geoscience Contributions, Targeted Geoscience Initiative, (ed.) P. K. Hannigan; Geological Survey of Canada, Bulletin 591, p. 195–219.

Abstract: Re-examination of the petrography and geochemistry of hydrothermal, fabric-destructive dolomite in the Pine Point area and in the subsurface to the southwest of Pine Point provides a basis for challenging the current model for dolomitization of the Presqu'ile barrier. Generally, saddle dolomite formed from high-salinity NaCl-$CaCl_2$ fluids and records no evidence of mixing with less-saline fluids. Late-stage calcite formed from less-saline NaCl fluids, suggesting minor mixing with less-saline, perhaps meteoric fluids that penetrated into these rocks after dolomitization.

Dolomitization may be related to extensional faults in the study area and the karstic pore-system that developed in the Presqu'ile barrier. The variability in the isotopic data can be explained by temporal or spatial variations in heat flow or the degree of recrystallization as a function of fluid-rock interaction.

Résumé : Un nouvel examen de la pétrographie et de la géochimie de la dolomite hydrothermale, destructrice de la pétrofabrique, dans la région de Pine Point et dans la subsurface au sud-ouest de Pine Point, sert de base pour contester le modèle courant de la dolomitisation de la barrière de Presqu'ile. En général, la dolomite en forme de selle s'est formée à partir de fluides de NaCl-$CaCl_2$ de forte salinité et ne témoigne aucunement de mélange avec des fluides moins salins. De la calcite de phase tardive s'est formée à partir de fluides de NaCl moins salins, ce qui donne à penser qu'il y a eu mélange de faible ampleur avec des fluides moins salins, possiblement d'origine météorique, qui ont pénétré dans ces roches après la dolomitisation.

La dolomitisation pourrait être associée à des failles d'extension dans la région à l'étude et au système karstique poreux qui s'est formé dans la barrière de Presqu'ile. La variabilité des données isotopiques peut être attribuée à des variations temporelles ou spatiales dans le flux thermique ou au degré de recristallisation en fonction de l'interaction fluide-roche.

[1] Department of Earth Sciences, University of Waterloo, Waterloo, Ontario N2L 3G1
[2] Geological Survey of Canada (Calgary), 3303-33rd Street N.W., Calgary, Alberta T2L 2A7
* Now at Talisman Energy Inc., Suite 3400, 888-3rd Street S.W., Calgary, Alberta, T2P 5C5, nwilson@talisman-energy.com

INTRODUCTION

The primary objective of this study is to present and interpret new data on the petrography, geochemistry, and temperature and composition of fluid inclusions of dolomite in the Middle Devonian succession of the southern portion of the Northwest Territories (NWT). These data allow us to test the robustness of the current paleohydrological model for the dolomitization of these rocks (Qing and Mountjoy, 1994a; Qing, 1998b). Furthermore, because their dolomitization and economic mineralization are closely related, these data also allow us to assess whether this model should guide predictions for the potential of these carbonate deposits to host Mississippi Valley-type (MVT) Pb-Zn deposits beyond the Pine Point property (e.g. Nelson et al., 2002).

Aspects of the geological setting of the Pine Point orebodies that made this deposit a world-class MVT style dolomite-hosted Pb-Zn camp, such as the abundance of faults (e.g. Morrow et al., 2006), also make correlative strata in the subsurface of NWT, Alberta and northeastern British Columbia (NEBC) excellent prospects for hydrocarbons (Griffin, 1967; Morrow et al., 2002; Morrow and Rhodes, 2001). This has led to considerable exploration activity in the subsurface of the Northwest and Yukon territories, Alberta and northeastern British Columbia (NEBC), and several important discoveries (e.g. Helmet, Peggo, July Lake, and Clarke Lake gas fields in NEBC; Pointed Mountain gas field in NWT and Kotaneelee gas field in Yukon).

These rocks comprise part of the Presqu'ile barrier, from its easternmost exposure in the Pine Point area, on the south side of Great Slave Lake, westward into the subsurface of the NWT, north of the Alberta boundary. The study site is located between latitudes 60°N and 62°N and longitude 120°W and 114°W, in the southern part of the NWT (Fig. 1). The study area includes the Pine Point Mines property.

The petrography and geochemistry of dolomite and late-stage calcite from the Pine Point area westward into the subsurface of the NWT and NEBC are described in detail in Qing's Ph. D. thesis (Qing, 1991), and several ensuing publications (Qing and Mountjoy, 1994a,b,c; Qing, 1998a,b). Other publications focusing on the stratigraphy, diagenesis and organic geochemistry of Pine Point orebodies include Skall (1975); Macqueen and Powell (1983); Medford et al. (1983); Krebs and Macqueen (1984); Rhodes et al. (1984); Mountjoy et al. (1992); and Fowler et al. (1993). Nelson et al. (2002) recently provided a comprehensive overview of the problem of age-dating the mineralization and dolomitization, and concluded that mineralization and dolomitization occurred during the Late Devonian.

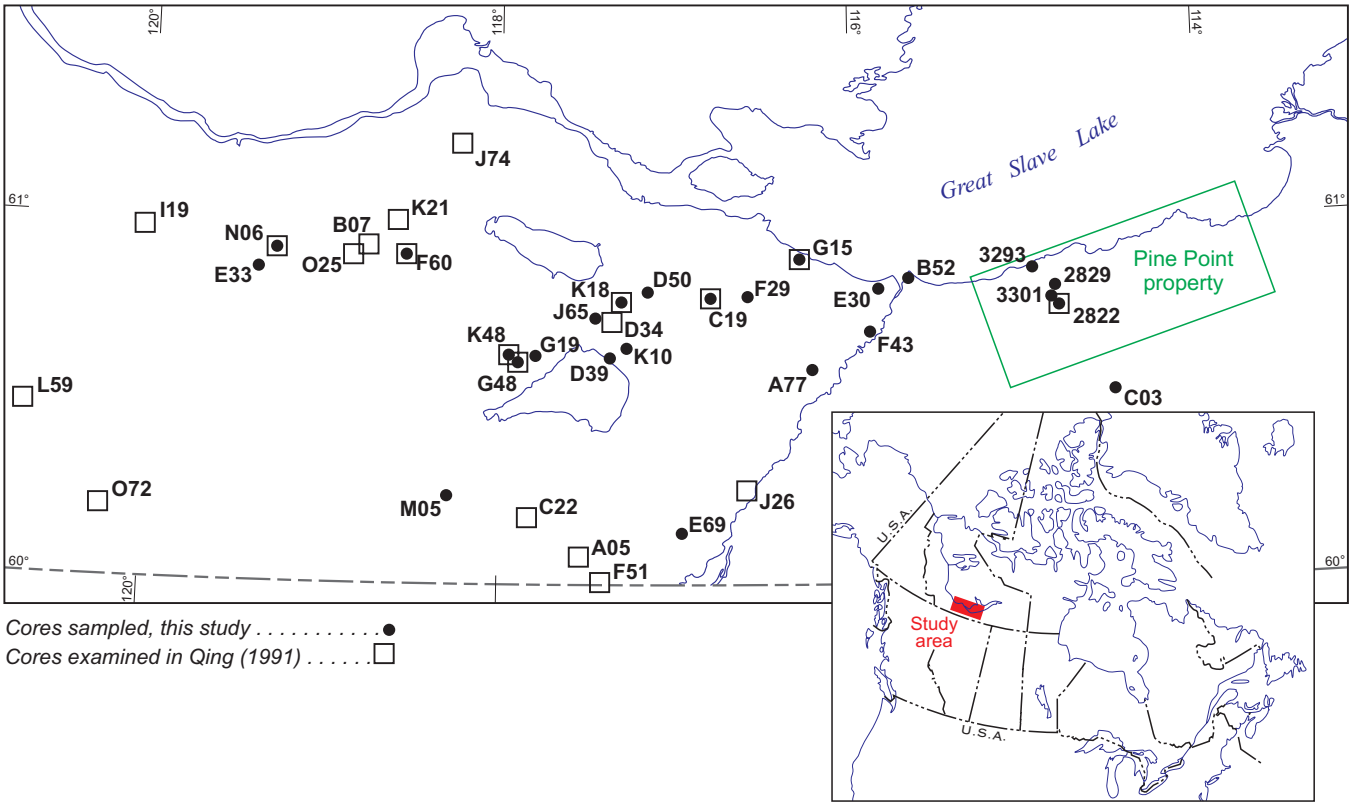

Figure 1. Locations of wells from which data used in this study were taken. Map also shows wells examined in NWT portion of Qing's (1991) study area.

STRATIGRAPHY AND GEOLOGICAL SETTING

The MVT deposits that comprise the Pine Point camp are hosted by paleokarstified rocks that were deposited as part of a Givetian (Middle Devonian) carbonate barrier complex – the Presqu'ile barrier – along the northern extremity of the Elk Point Basin of the Western Canada Sedimentary Basin (Morrow and Rhodes, 2001). This barrier is at least 400 km in length and ranges from 20 to 100 km in width (Qing, 1998a). Middle Devonian carbonate deposits in the area of Pine Point reach a maximum thickness of 300 m. Correlative strata occur in the subsurface to the west and south of Pine Point, extending into NEBC and northern Alberta, where they reach depths of 2000 to 2300 m (Qing, 1998a).

The strata forming the barrier complex existed as a bathymetric high that separated the rapidly subsiding, largely evaporitic Elk Point Basin to the south from open-marine conditions to the north (Morrow and Rhodes, 2001). This study focuses on the carbonate strata associated with the Presqu'ile barrier complex, as they occur both on the Pine Point property and in correlative rocks in the subsurface from the southern part of the NWT. Of particular interest are the Lower Keg River Member, which forms the regional platform on which the barrier developed; the Pine Point Formation (also referred to as Upper Keg River Member) and the Sulphur Point Formation, which together comprise the barrier complex; and the overlying Slave Point Formation. The stratigraphic nomenclature of the Presqu'ile barrier carbonate deposits that are laterally equivalent to the Muskeg Formation has been the subject of some controversy. For consistency, we have adopted the terminology used by most authors in this bulletin and use "Pine Point Formation" in place of upper Keg River Member. A recent discussion on the stratigraphic terminology as it relates to the Presqu'ile barrier and associated and correlative strata and the many inconsistencies in previous usage of the term "Pine Point Formation" is presented in Morrow et al. (2002). Here, we follow the usage of Rhodes et al. (1984) for the term "Pine Point Formation".

The stratigraphy in the area of the Pine Point Mines property is documented in detail by Rhodes et al. (1984) and references therein (Fig. 2). At Pine Point, however, the lateral continuity of beds is commonly disrupted by crosscutting tabular and prismatic Pb-Zn bodies, thus complicating interpretation of the lithostratigraphy (Morrow et al., 2006).

The Lower Keg River Member is an areally extensive unit averaging 65 m in thickness, and composed mostly of dolomitized crinoidal and brachiopod wackestone deposited in a shallow-marine setting (Rhodes et al., 1984). The Lower Keg River Member is overlain by the Presqu'ile barrier, the lower two-thirds of which consists of the Pine Point Formation (or Upper Keg River Member), which is composed of a diverse assemblage of limestone and dolomite facies, including bioclastic grainstone, packstone, rudstone and floatstone,

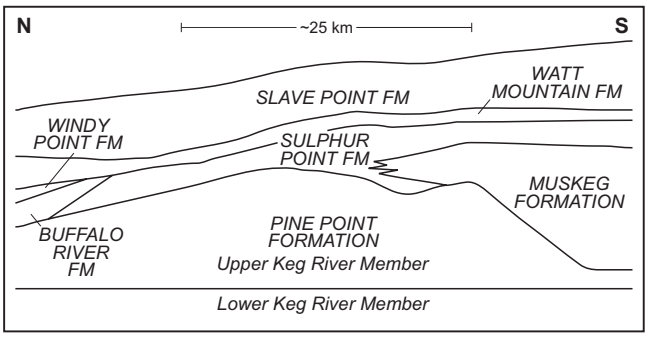

Figure 2. Schematic cross-section showing stratigraphy of the Presqu'ile barrier in the western part of the Pine Point property. Diagram is *modified from* Qing and Mountjoy (1994a).

wackestone and mudstone. This lenticular unit reaches 175 m in thickness at the middle of the barrier, but thins toward the north and south. The rest of the Presqu'ile barrier is composed of the Sulphur Point Formation, which consists of limestone and dolomite that reach 65 m in thickness. The spectrum of depositional facies in the Sulphur Point Formation is similar to those of the underlying Pine Point Formation, but these strata are differentiated from the Pine Point Formation by their lighter colour.

The Pine Point and Sulphur Point formations pass laterally to the south into back-barrier evaporite and interbedded dolomite of the Muskeg Formation. North of the barrier, open-marine conditions led to deposition of carbonate and shale of the Buffalo River Formation (Morrow and Rhodes, 2001). These rocks are unconformably overlain by the Watt Mountain Formation, which averages less than 10 m in thickness and consists of marl and shale overlain by interbedded limestone, dolomite and shale (Morrow and Rhodes, 2001). This unit is considered to be a regional aquiclude (Morrow et al., 2002). The succeeding Slave Point Formation conformably overlies the Watt Mountain Formation and consists of argillaceous limestone and variably fossiliferous, mostly muddy, limestone (Rhodes et al., 1984).

Qing (1991) used stratigraphic information and geothermal indicators to conclude that maximum burial of this succession occurred during the Late Cretaceous to early Tertiary. Maximum burial depths were estimated to be 3500 to 4000 m in NEBC, 2000 to 3500 m in NWT and 1500 m in the Pine Point area. The present-day depths of the Presqu'ile barrier are approximately 2000 to 2500 m in NEBC and approximately 1500 to 2000 m in the NWT north of the Alberta–BC boundary.

The diagenetic history of the rocks of the Presqu'ile barrier is well described in Krebs and Macqueen (1984), Qing (1991 and ensuing journal publications) and Morrow et al. (2002). These rocks record alteration in submarine, subaerial and especially subsurface environments, where compaction, fracturing, pressure solution, several stages of calcite and dolomite precipitation, sulphide mineralization and bitumen emplacement occurred (Fig. 3).

The Phanerozoic section is dominated by prominent northeast-trending, mostly extensional faults, showing varying amounts of offset (Morrow et al., 2006; MacLean, 2006). This dominant trend, which includes the Rabbit Lake structure, Tathlina Fault, and the Hay River Fault Zone is parallel to the Great Slave Shear Zone (Fig. 4) and, with the less prominent northwest-trending set, results in an orthogonal structural grain that affected the entire Paleozoic section, and is expressed from the Precambrian basement to the present-day surface. Basement faults apparently also played a role in locating the Middle Devonian carbonate bank edge, as suggested by the position and orientation of the carbonate-to-shale transition line (MacLean, 2006). Furthermore, MacLean (2006) suggested that the structural grain had an effect on the development of hydrothermal dolomite, although the spatial relationships are ambiguous. The location of wells containing saddle dolomite that were examined in this study, at least in the southwestern part of the study area in Figure 4, appear to trend along some of the northeast-trending faults, but an equal number of wells occur away from the faults. The connection between zones of weakness and dolomitization, however, seems more convincing in the eastern part of the study area (Janicki, 2006), particularly near the Hay River Fault Zone, which is parallel to the orientation of Pine Point orebodies (Krebs and Macqueen, 1984; Nelson et al., 2002).

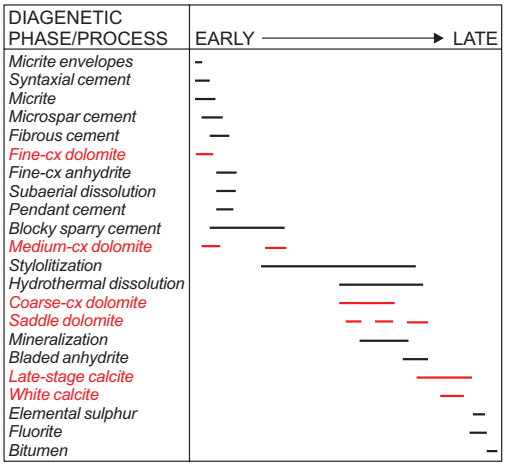

Figure 3. Paragenesis of diagenetic phases and events of the Presqu'ile barrier. Cx = crystalline. *From* Qing and Mountjoy (1994a). Phases discussed in this report are in red.

METHODOLOGY

Core examination and sampling

This study is based on four diamond-drill cores from the Pine Point Mines property and 31 petroleum cores from the subsurface of the NWT to the west of Pine Point (Fig. 1, Tables 1, 2). All cores were examined at the Geological Survey of Canada (Calgary) core storage facility. Twenty-one petroleum cores and the four diamond-drill cores were sampled, from which 91 polished thin sections and 25 doubly polished fluid inclusion sections were made. Petrographic analysis under transmitted light was carried out on a conventional Nikon microscope and under cathodoluminescence using a Technosyn 8200 Cold Cathode Luminoscope operating at 15 to 17 kV beam voltage and 0.7 to 0.8 mA beam current. Thin sections were subsequently stained with Alizarin Red S and potassium ferricyanide solution. Stained thin sections revealed that dolomite extracted for chemical

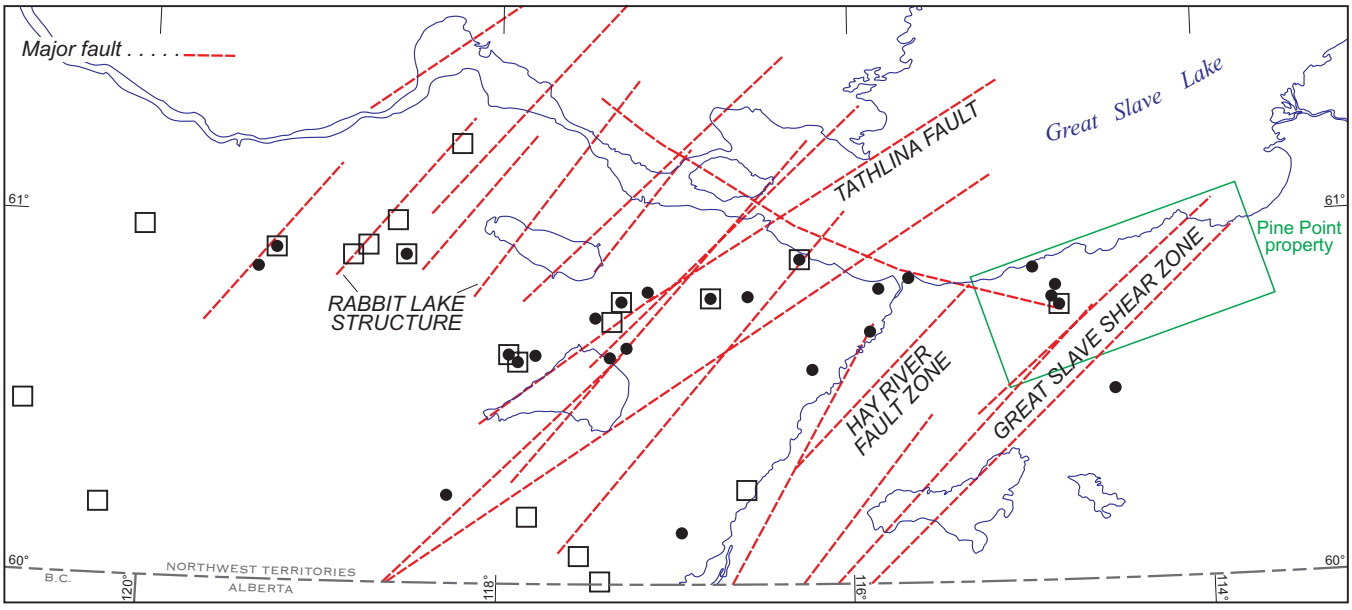

Figure 4. Major faults in the study area. Fault locations are from Morrow et al. (2006). Well symbols as in Figure 1.

Table 1. Cored boreholes examined in this study

Well Name	Well location	Well location (NAD 83)	UTM (NAD 83)
NWT Escarpment Lake #3 A-77	A-77/60-40-116-00	60 36 05.43; 116 13 23.05	542532E; 6718653N; 11
Horn River et al. Hay River B-52	B-52/61-00-115-30	60 51 04.46; 115 40 21.89	572118E; 6746948N; 11
CDR Wood Buffalo 2 C-03	2C-03/60-40-114-30	60 32 07.95; 114 31 14.85	636022E; 6713619N; 11
NWT Desmarais Lake #1 C-19	C-19/60-50-116-45	60 48 00.41; 116 48 05.05	510809E; 6740540N; 11
Briggs Feotus Lake #1 D-06 (aka F-50 or F-60)	D-06/61-00-118-30	60 55 13.22; 118 31 53.97	416957E; 6754834N; 11
Calstan Tathlina Lake D-39	D-39/60-40-117-15	60 38 01.39; 117 22 25.09	479559E; 6722049N; 11
Placid Chevron NE Tathlina D-50	D-50/60-50-117-00	60 49 06.90; 117 09 13.48	491637E; 6742590N; 11
General Crude Ranvik Hay River E-30	E-30/60-50-115-45	60 49 23.97; 115 50 34.70	562924E; 6743664N; 11
Wilkinson Redknife River No. 2 E-33	E-33/61-00-119-15	60 52 29.34; 119 22 28.21	371087E; 6751178N; 11
Canso et al. North Cameron Hills E-69	E-69/60-10-116-45	60 08 24.63; 116 57 52.84	501962E; 6667023N; 11
NWT Heart Lake #1 F-29	F-29/60-50-116-30	60 48 18.42; 116 35 11.04	522507E; 6741152N; 11
Frobisher Hay River #8 F-43	F-43/60-50-115-45	60 42 22.45; 115 53 53.92	560133E; 6730571N; 11
General Crude Ranvik Reef Creek G-15	G-15/61-00-116-15	60 54 24.44; 116 17 34.99	538347E; 6752612N; 11
Briggs West Tathlina No. 2 G-19	G-19/60-40-117-45	60 38 08.08; 117 47 32.42	456656E; 6722459N; 11
Briggs West Tathlina #1 G-48	G-48/60-40-117-45	60 37 21.68; 117 53 13.23	451458E; 6721089N; 11
Placid Chevron Kakisa J-65	J-65/60-50-117-15	60 44 42.40; 117 27 12.07	475284E; 6734482N; 11
Calstan Tathlina Lake K-10	K-10/60-40-117-15	60 39 40.59; 117 16 25.37	485039E; 6725091N; 11
Briggs NE Tathlina Lake K-18	K-18/60-50-117-15	60 47 35.90; 117 18 02.37	483633E; 6739803N; 11
Placid Wood West Tathlina K-48	K-48/60-40-117-45	60 37 36.38; 117 53 45.13	450980E; 6721551N; 11
Pacific Phillip N Cameron Hills M-05	M-05/60-20-118-15	60 14 57.89; 118 16 52.19	429081E; 6679877N; 11
Imperial Redknife N-06	N-06/61-00-119-15	60 55 49.36; 119 16 15.18	376926E; 6757165N; 11
NWT Escarpment Lake #1 L-66	2L-66/60-40-116-00	60 35 43.43; 116 13 04.95	542829E; 6717977N; 11
Briggs Tathlina Lake #7 D-44 (also J-53)	J-53/60-50-117-15	60 42 33.39; 117 24 05.08	478091E; 6730473N; 11
MCD et al. Sulphur Point #1 O-07	O-07/61-00-114-45	60 56 57.50; 114 45 34.64	621349E; 6759215N; 11
NWT Heart Lake #2 I-41	I-41/61-00-116-30	60 50 30.42; 116 37 35.05	520307E; 6745222N; 11
Murphy Alexandra Falls #2 J-26	J-26/60-20-116-30	60 15 31.20; 116 34 44.99	523290E; 6680293N; 11
Pan Am-Shell Kakisa F-35	F-35/61-00-117-15	60 54 25.41; 117 21 54.07	480200E; 6752490N; 11
HB Cameron Hills F-51	F-51/60-10-117-15	60 00 15.80; 117 25 36.67	476194E; 6651977N; 11
CPOG Chevron Tathlina K-24	K-24/60-40-118-00	60 33 39.73; 118 05 03.47	440549E; 6714385N; 11
Briggs NE Tathlina Lake #9 D-34	D-43/60-50-117-15	60 43 12.40; 117 22 22.08	479660E; 6731670N; 11
Briggs Tathlina Lake #3 F-01	F-01/60-50-117-30	60 40 29.88; 117 31 14.66	471548E; 6726697N; 11
Diamond-drill Hole Name	**NTS**	**DDH location (NAD 83)**	**UTM (NAD 83)**
Pine Point DDH # 2822	85B/15	60 45 44.33; 114 49 48.16	618225E; 6738267N; 11
Pine Point DDH # 2829	85B/15	60 48 37.81; 114 50 19.44	617575E; 6743617N; 11
Pine Point DDH # 3293	85B/15	60 51 49.16; 114 57 50.68	610574E; 6749317N; 11
Pine Point DDH # 3301	85B/15	60 46 52.66; 114 51 55.87	616224E; 6740317N; 11

Table 2. Petrographic and geochemical data

Dolomite Samples[1]								
Thin section number	**Core/depth (m)**	**Dolomite types**	**Sample number**	**Formation**	**$\delta^{13}C$ ‰**	**$\delta^{18}O$ ‰**	**$^{87}Sr/^{86}Sr$**	**Estimated crystal size**
PETROGRAPHIC DATA FOR SAMPLES WITH ISOTOPE ANALYSIS								
10	A-77-469.4	SD	C-421064-A	Sulphur Point	-0.9	-11.2		1–5 mm
14	A-77-470.6	SD	C-421065-B	Sulphur Point	-0.8	-10.5		up to 2.5 mm
19	B-52-172.0	SD	C-421067	Watt Mountain	1.5	-13.0	0.708168	up to 5 mm
17	C-19-477.5	SD	C-421069-A	Slave Point	2.4	-11.9	0.708768	200 µm–6 mm
20	D-39-753.4	SD	C-421072	Slave Point	2.7	-9.0	0.708487	400–5000 µm
23	E-30-228.4	SD	C-421077-A	Sulphur Point	1.9	-9.9		up to 6 mm
27	F-29-490.1	SD	C-421082-A	Pine Point	1.5	-9.1	0.708237	800–5000 µm
28	F-29-491.0	SD	C-421083-A	Pine Point	1.6	-8.4		6 mm
31	G-15-271.9	SD	C-421085-A	Sulphur Point	0.8	-12.1		up to 15 mm blades
32	G-15-279.8	SD	C-421086-A	Sulphur Point	0.6	-11.6		up to 3.2 mm
35	G-19-962.0	SD replacement (cement?)	C-421089	Lower Keg River	-0.9	-11.2		800–2000 µm
37	G-48-964.7	SD	C-421091-B	Lower Keg River	0.7	-8.7		up to 800 µm
44	M-05-1278.6	SD	C-421100-A	Pine Point (limestone)	-0.3	-10.1	0.709085	up to 2.4 mm
46	N-06-974.2	SD	C-421102	Pine Point	0.4	-10.4	0.708547	up to 3.5 mm
47	2822-88.6	SD	C-421111	Sulphur Point	0.4	-10.0		up to 4 mm
48	2822-100.3	SD	C-421115-B	Sulphur Point	0.3	-10.9		2–3 mm
49	2822-109.6	SD	C-421119	Muskeg	1.0	-10.1	0.70833	100–400 µm, cement up to 4 mm
50	2822-112.4	SD	C-421120	Muskeg	1.7	-7.2		80–2400 µm
52	2822-113.0	SD	C-421121-B	Muskeg	0.8	-8.4		80–2000 µm
56	2829-81.3	SD	C-421130-B	Sulphur Point	0.0	-10.7		up to 4 mm, elongate
59	3293-98.8	SD	C-421141-A	Windy Pt Fm	2.5	-11.5		0.8–2 mm
62	3293-206.3	SD	C-421144-B	Lower Keg River	11.8	-8.0		up to 1.2 mm
63	3301-88.6	SD	C-421149-A	Sulphur Point	0.2	-10.0		up to 4 mm
65	3301-88.8	SD	C-421150-A	Sulphur Point	0.1	-10.5	0.708188	up to 4 mm
11	A-77-469.4	WTGD	C-421064-B	Sulphur Point	-0.8	-11.1		400 µm to 2 mm
13	A-77-470.6	WTGD	C-421065-A	Sulphur Point	-0.9	-10.3		80–600 µm
22	D-50-579.5	WTGD	C-421074	Slave Point	2.2	-10.8		80–400 µm
30	F-43-264.7	WTGD	C-421084	Sulphur Point	0.3	-9.1	0.708494	200–800 µm
33	G-15-279.8	WTGD	C-421086-B	Sulphur Point	0.7	-11.3		400–1200 µm, up to 2.8 mm
38	J-65-793.6	WTGD	C-421093	Sulphur Point	1.5	-12.4	0.708408	200–800 µm
39	K-10-704.4	WTGD	C-421094-A	Slave Point	1.9	-11.8	0.708573	200–600 µm
53	2822-214.9	WTGD	C-421125	Pine Point	3.2	-4.1	0.70851	30–100 µm
55	2829-81.3	WTGD	C-421130-A	Sulphur Point	0.1	-10.5		400 µm to 4 mm
64	3301-88.6	WTGD	C-421149-B	Sulphur Point	0.3	-10.6		80–800 µm
66	3301-88.8	WTGD	C-421150-B	Sulphur Point	0.2	-9.7		400–1000 µm +
41	K-10-706.1	MDGD	C-421095	Slave Point	1.8	-13.2		200–800 µm
12	A-77-469.4	MDGD	C-421064-C	Sulphur Point	-0.8	-11.6		800 µm to 2 mm

[1]SD = saddle dolomite; WTGD = White to tan-grey dolomite; MDGD = Medium to dark grey dolomite

Table 2. (cont.)

Dolomite Samples								
Thin section number	**Core/depth (m)**	**Dolomite types**	**Sample number**	**Formation**	**$\delta^{13}C$ ‰**	**$\delta^{18}O$ ‰**	**$^{87}Sr/^{86}Sr$**	**Estimated crystal size**
PETROGRAPHIC DATA FOR SAMPLES WITH ISOTOPE ANALYSIS								
15	A-77-470.6	MDGD	C-421065-C	Sulphur Point	-0.8	-10.5		80–600 µm
18	C-19-477.5	MDGD	C-421069-B	Slave Point	2.3	-12.4		80–600 µm
21	D-50-575.2	MDGD	C-421073	Slave Point	2.0	-11.2	0.70846	80–200 µm
24	E-30-228.4	MDGD	C-421077-B	Sulphur Point	1.4	-10.0	0.708296	80–400 µm
25	E-69-888.8	MDGD	C-421080	Pine Point	2.6	-7.0	0.708161	400–1200 µm
26	E-69-891.2	MDGD	C-421081	Pine Point	2.1	-2.0		160–400 µm
29	F-29-491.0	MDGD	C-421083-B	Pine Point	1.5	-8.8		200–800 µm, some up to 4 mm
34	G-15-284.1	MDGD	C-421087	Sulphur Point	1.4	-11.7	0.708306	200 µm–1.2 mm, some sub-xl patches up to 4 mm
36	G-48-964.7	MDGD	C-421091-A	Lower Keg River	0.7	-7.3	0.708922	80–400 µm
40	K-10-704.4	MDGD	C-421094-B	Slave Point	1.9	-12.0	0.711193	30–100 µm, locally up to 600 µm
42	K-18-746.6	MDGD	C-421096	Lower Keg River	1.2	-8.6	0.708901	30–100 µm, up to 200 µm near pores
43	K-18-750.3	MDGD	C-421097	Lower Keg River	-0.7	-0.8		5–15 µm
45	M-05-1278.6	MDGD	C-421100-B	Pine Point (limestone)	0.0	-4.0	0.708361	20–50 µm
51	2822-113.0	MDGD	C-421121-A	Muskeg	0.7	-8.8		400–1200 µm
57	2829-105.5	MDGD	C-421133	Pine Point	1.4	-7.9	0.708301	200–600 µm=matrix; SD cement lining pores=1.2 mm
58	3293-47.2	MDGD	C-421138	Slave Point	0.6	-10.8	0.709324	30–100 µm
61	3293-206.3	MDGD	C-421144-A	Lower Keg River	2.1	-8.0		80–200 µm
67	3301-234.4	MDGD	C-421159	Pine Point	2.7	-1.9		up to 200–300 µm on pore-filling, mostly 50–70 µm
16	B-52-171.1	Sucrosic dolomite	C-421066	Watt Mountain	1.5	-12.7	0.708521	400 µm to 2 mm mostly, some up to 6 mm
54	2829-45.4	Sucrosic dolomite	C-421129	Slave Point	0.5	-8.6		10–30 µm
60	3293-98.8	Sucrosic dolomite	C-421141-B	Windy Pt Fm (below Wt Mtn)	2.4	-11.7		50–100 µm, locally 200–400 µm , some up to 4 mm
PETROGRAPHIC DATA: NO ISOTOPE ANALYSIS								
	D-50-579.8	breccia mtx	C-421075	Slave Point				200–400 µm
	2822-42.0	dispersed dolomite	C-421106	Slave Point limestone				50–100 µm
	2822-50.6	dispersed dolomite	C-421107	Slave Point limestone				15–20 µm
	2822-55.1	dispersed dolomite	C-421108	Slave Point limestone				10–20 µm
	2828-33.9	dispersed dolomite	C-421128	Slave Point limestone				80–120 µm

Table 2. (cont.)

Dolomite Samples								
Thin section number	**Core/depth (m)**	**Dolomite types**	**Sample number**	**Formation**	**$\delta^{13}C$ ‰**	**$\delta^{18}O$ ‰**	**$^{87}Sr/^{86}Sr$**	**Estimated crystal size**
PETROGRAPHIC DATA: NO ISOTOPE ANALYSIS								
	3293-18.7	dispersed dolomite	C-421136	Slave Point limestone				20–30 µm
	3293-28.5	dispersed dolomite	C-421137	Slave Point limestone				100–200 µm
	3293-97.0	dispersed dolomite	C-421140	Windy Point limestone				
	3301-49.4	dispersed dolomite	C-421145	Slave Point limestone				up to 400 µm
	3301-59.2	dispersed dolomite	C-421146	Slave Point limestone				30–70 µm, SD up to 800 µm
	3301-85.1	dispersed dolomite	C-421148	Sulphur Point limestone				SD up to 800 µm
	D-50-579.8	SD	C-421075	Slave Point				
	G-15-284.1	SD	C-421087	Sulphur Point				400–800 µm
	G-19-962.0	SD	C-421088	Lower Keg River				up to 2.4 mm
	J-65-793.6	SD	C-421093	Sulphur Point				up to 2.5 mm
	K-10-704.4	SD	C-421094	Slave Point				
	K-48-938.8	SD	C-421098	Pine Point				up to 6 mm
	K-48-942.1	SD	C-421099	Pine Point				up to 6 mm
	N-06-974.3	SD	C-421103	Pine Point				up to 8 mm
	2822-83.9	SD	C-421109	Sulphur Point				up to 4 mm
	2822-87.1	SD	C-421110	Sulphur Point				up to 4 mm
	2822-88.6	SD	C-421112	Sulphur Point				
	2822-106.4	SD	C-421118	Sulphur Point				cement up to 3.2 mm, repl 800–3200 µm
	2822-120.3	SD	C-421122	Muskeg				40–1200 µm, rarely up to 4 mm
	2829-90.9	SD	C-421131	Sulphur Point				200–2800 µm
	3301-129.0	SD	C-421152	Muskeg				
	3301-135.3	SD	C-421153	Pine Point				400–3200 µm
	3301-142.0	SD	C-421154	Pine Point				800–2000 µm
	C-03-102.5	WTGD	C-421068	Sulphur Point				variable
	G-48-963.5	WTGD	C-421090	Lower Keg River				50–500 µm
	2822-140.3	WTGD	C-421123	Muskeg				80–200 µm, few SD up to 1.2 mm
	2822-163.2	WTGD	C-421124	Pine Point				120–200 µm
	3301-135.3	WTGD	C-421153	Pine Point				250–1500 µm
	3301-142.0	WTGD	C-421154	Pine Point				80–800 µm
	B-52-172.0	MDGD	C-421067	Watt Mountain				50–400 µm
	C-19-478.5	MDGD	C-421070	Slave Point				160–400 µm
	E-30-225.7	MDGD	C-421076	Sulphur Point				400–1200 µm
	K-48-942.1	MDGD	C-421099	Pine Point				50–100 µm
	M-05-1286.0	MDGD	C-421101	Pine Point				80–120 µm

[1]SD = saddle dolomite; WTGD = White to tan-grey dolomite; MDGD = Medium to dark grey dolomite

Table 2. (cont.)

Dolomite Samples								
Thin section number	Core/depth (m)	Dolomite types	Sample number	Formation	$\delta^{13}C$ ‰	$\delta^{18}O$ ‰	$^{87}Sr/^{86}Sr$	Estimated crystal size
PETROGRAPHIC DATA: NO ISOTOPE ANALYSIS								
	2822-100.3	MDGD	C-421116	Sulphur Point				200–600 µm, some cement up to 800 µm
	2829-130.9	MDGD	C-421134	Pine Point				80–120 µm
	3301-212.5	MDGD	C-421156	Pine Point				50–100 µm, pore lining crystals up to 200 µm
	3301-223.2	MDGD	C-421158	Pine Point				30–50 µm
	3301-262.2	MDGD	C-421160	Pine Point				50–100 µm
	N-06-974.9	Sucrosic dolomite	C-421104	Pine Point				up to 6 mm, most 800–1200 µm
	2822-100.3	Sucrosic dolomite	C-421115	Sulphur Point				80–400 µm, up to 1–2 mm
	2822-242.5	Sucrosic dolomite	C-421126	Pine Point				20–30 µm
	2822-246.4	Sucrosic dolomite	C-421127	Pine Point				30–50 µm
	2829-216.4	Sucrosic dolomite	C-421135	Pine Point				20–50 µm
	3293-190.7	Sucrosic dolomite	C-421143	Pine Point				40–80 µm
Calcite samples								
1	C-19-478.5	Calcite	C-421070	Slave Point	-17.4	-8.1		
2	F-29-490.1	Calcite	C-421082-B	Pine Point	-4.4	-10.4	0.715513	
3	F-29-491.0	Calcite	C-421083-C	Pine Point	-5.8	-8.6		
4	G-15-271.9	Calcite	C-421085-B	Sulphur Point	-7.6	-6.6		
5	2822-50.6	Calcite	C-421107	Slave Point	-2.7	-15.3		
6	2822-100.3	Calcite	C-421115-A	Sulphur Point	-1.3	-7.0		
7	2822-103.7	Calcite	C-421117	Sulphur Point	3.0	-4.9	0.713374	
8	3301-75.9	Calcite (fibrous marine)	C-421147	Sulphur Point	2.2	-4.9		
9	3301-135.3	Calcite	C-421153	Pine Point	-5.2	-9.4		

analysis was essentially pure with few exceptions. Care was taken to ensure that extraneous components (e.g. evaporite and late-stage calcite cements) were not included.

Carbon and oxygen isotopic data

A total of 67 samples of carbonate (58 dolomite, 9 calcite) were extracted for stable carbon and oxygen isotopic analysis using a modified dental drill. Samples were pretreated by roasting at 470°C using a helium flow for 45 minutes to remove volatile organics. Samples were analyzed at the Isotope Science Laboratory in the Department of Physics and Astronomy at the University of Calgary. Approximately 10 to 20 mg of untreated powder was reacted with 100% phosphoric acid at 25°C. All dolomite samples were subject to a two-stage procedure whereby CO_2 from any possible calcite was produced after the first 3 to 5 hours and then frozen in a 6 mm breakseal vessel. After a further 48 hours, the remaining CO_2 from dolomite was sealed in a second breakseal vessel. Only the results from the second stage of analysis are reported for dolomite.

The evolved CO_2 gas was analyzed for $^{18}O/^{16}O$ and $^{13}C/^{12}C$ using a VG 903 dual inlet isotope mass spectrometer. Results are reported in conventional per mil notation relative to PDB, using standard correction procedures. No correction for acid fractionation was made for dolomite. Precision, based on replication of international and internal standards, is ±0.2 and ±0.3 ‰ for C and O, respectively.

Strontium isotopic data

Dolomite (n = 23) and calcite (n = 2) were analyzed for $^{87}Sr/^{86}Sr$ ratios at the Radiogenic Isotope Facility at the University of Alberta. Powders were dissolved in dilute cold

(approx.0.75N) HCl to minimize any Sr release from potential contaminant silicate phases, such as clays. After centrifugation, Sr was separated by conventional cation exchange chromatography, and the isotopic composition determined by Thermal Ionization Mass Spectrometry (TIMS). All data are normalized for instrumental fractionation to a value of $^{86}Sr/^{88}Sr = 0.1194$ and are presented relative to a value of 0.710245 for the NIST Standard Reference Material SRM987 Sr isotope standard. Uncertainty in $^{87}Sr/^{86}Sr$ is expressed as ± 2 sigma of the mean, equivalent to two standard errors (2SE).

Fluid inclusion petrography and microthermometry

Prior to petrographic study, images of the doubly polished thin sections (100 µm) were created using a Canon FS slide scanner. Fluid inclusion petrography was performed at 25°C where inclusion types, distribution, origin, and relative age of inclusions were determined and mapped on the section images. Fluid inclusion assemblages (FIAs) were identified based on criteria of Goldstein and Reynolds (1994) and measurements were made on primary two-phase liquid + vapour (5–10% vapour bubble) inclusions aligned along growth zones, and secondary inclusions with similar liquid-vapour ratios along fracture planes.

Homogenization (T_h) and ice melting (T_m) temperatures were collected using a Linkam THMSG 600 heating and freezing stage mounted on a Zeiss Axioplan II microscope controlled by a CI 93 programmer, LNP cooling pump, and LinkSys software. Synthetic fluid inclusions were used to calibrate the stage at 374.1°C, 0.0°C, and -56.6°C. The samples (chips) were not removed from the glass mounting slides during microthermometry. Freezing studies were conducted after heating studies and ice-melting temperatures (T_m) were converted to weight per cent NaCl equivalent after Bodnar (1993).

DOLOMITIZATION: PREVIOUS WORK

Overview of previous petrographic studies

Most of the carbonate deposits in the Pine Point area are dolomite, however limestone becomes increasingly common in the more argillaceous and bituminous strata in the Pine Point Formation (Morrow and Rhodes, 2001). The distribution and petrographic characteristics of dolomite in the Pine Point area and equivalent strata in the subsurface are summarized below from Qing (1991) and the subsequent publications arising from this work (Table 3).

According to Qing (1991), four types of dolomite are associated with the Presqu'ile barrier: 1) FCD (fine-crystalline dolomite) and 2) MCD (medium-crystalline dolomite), which were the focus of Qing (1998a); and 3) CCD (coarse-crystalline dolomite) and 4) SD (saddle dolomite) which were examined in Qing and Mountjoy (1994a). MCD is the dominant dolomite type in these rocks.

CCD is generally referred to as Presqu'ile dolomite (e.g. Krebs and Macqueen, 1984) and is typical of the dolomite deposits that host many other MVT deposits (e.g. Leach and Sangster, 1993). This style of replacive dolomitization is mostly fabric destructive, although coarser depositional components can sometimes be recognized. This fabric is characteristically vuggy, fractured and brecciated. CCD sometimes displays distinctive "subrounded forms", interpreted as scattered nucleation sites in the precursor limestone, which includes a wide variety of depositional facies (Morrow and Rhodes, 2001). Coarse white SD cement is the last phase of dolomitization associated with Presqu'ile dolomite or can occur as a later, void-filling and replacement phase (Morrow and Rhodes, 2001). CCD and SD occur in multiple phases (Krebs and Macqueen, 1984) – SD can predate, be synchronous with, or postdate sulphide mineralization. There is a close spatial association between the Presqu'ile dolomite and mineralization, although this type of dolomitization is significantly more widespread in outcrop and subsurface than sulphide mineralization. Detailed descriptions of the fabrics associated with mineralization can be found in Krebs and Macqueen (1984) and Qing (1991 and subsequent journal publications). MCD and CCD are probably linked genetically, based on some overlap of the distribution of these two types of dolomite, and MCD can be seen to pass gradationally into CCD (Morrow and Rhodes, 2001).

Qing (1991) also identified two types of late-stage, coarse crystalline calcite in these rocks, which he referred to as "late-stage coarse-crystalline calcite" and "white calcite" (WCC). The former is widespread throughout his study area. These calcite crystals occur as rhombohedra or hexagonal scalenohedra, which vary from a few millimetres to approximately 20 cm in size, and they postdate saddle dolomite and sulphide minerals. WCC occurs as anhedral mosaics in 1–5 cm-thick bands between layers of saddle dolomite cement. Qing (1991) indicated that this phase was previously misidentified by earlier authors as saddle dolomite. This phase, which Qing (1991) interpreted as dedolomite, locally replaces the early stage of some saddle dolomite, and retains typical saddle dolomite textures, making it difficult to distinguish. Qing (1991) noted that dedolomite occurs only at Pine Point and is associated closely with orebodies.

Isotopes

Previous work on carbon isotopes in the spectrum of dolomites recognized did not reveal any spatial or stratigraphic trends. $\delta^{13}C$ values reported in Qing (1991) range from -3.7 to +2.5‰ (Fig. 23 *in* Qing, 1991). Qing (1991) concluded that the dominant carbon input into these dolomite deposits would have been generated from inorganic carbon recycled from Middle Devonian marine limestone. Qing and Mountjoy (1994a) further suggested that $\delta^{13}C$ values for SD

Table 3. Dolomite characteristics in Presqu'ile Barrier (*summarized from* Qing and Mountjoy, 1994a; Qing, 1998a)

Dolomite type	Petrography	Associations/ occurrence	$\delta^{18}O$	$^{87}SR/^{86}SR$	Fluid inclusions
FCD	• brown or grey • subhedral to euhedral • 5–25 µm size, increasing to 100 µm toward ore bodies • fossils and sedimentary structures are well preserved	• present only in back-barrier facies of Muskeg Fm	• -1.6 to -3.8‰; • mean = -2.8‰ • -6.7 to -7.9‰ for altered FCD • mean = -7.3‰	• 0.7079–0.7081 • mean = 0.7080 • 0.7082–0.7083 for altered FCD • mean = 0.7083	• no data
MCD	• medium to dark brown • anhedral to subhedral crystals, some with clear rims toward pore centres • 150–250 µm, mean 200 µm • plane extinction • fossils and sedimentary structures are generally recognizable • red to orange CL with bright orange blotches along some crystal boundaries • vugs and fractures locally developed • variable intra- and intercrystalline porosity	• forms lower part of Presqu'ile barrier	• -3.7 to -9.4‰ • mean -5.9‰	• 0.7081–0.7087 • mean 0.7084	• no data
CCD	• light brown or buff • subhedral to anhedral crystals • 500 µm – 2 mm • undulatory extinction • uniform, dull red CL • vugs and fractures commonly contain SD and host MVT minerals at PP and create reservoir rocks in NWT and NEBC • crystals contain 2–5 µm intracrystalline dissolution pores • original sedimentary fabrics mostly destroyed • replaces limestone	• mostly Sulphur Point Fm, some extends above Watt Mountain unconformity	• -7.9 to -15.8‰ • mean = -11.7‰	• 0.7082 –0.7121 • mean = 0.7095	• no data
SD	• distinctive white colour in hand specimen, locally pink or gray • rhombohedral to symmetrical saddle forms • strong undulatory extinction • uniform bright orange cathodoluminescence (Qing and Mountjoy, 1994a) vs. uniform dull red luminescence and some SD has deeper red cores and brighter red rims (Qing, 1991) • some CL zoning but is not regionally correlatable	• cement associated with CCD • mostly Sulphur Point Fm, some extends above Watt Mountain unconformity	• -7.0 to -16.0‰ • mean = -10.4‰	• 0.7081–0.7106 • mean = 0.7087	• T_h of primary inclusions ranges from 92–178°C • T_m -7 to -28°C; calculated salinities = 10–28% NaCl • T_e -31 to -65°C; fluid dominantly NaCl and $CaCl_2$ with subordinate KCl and $MgCl_2$

and CCD (+1.7 to -3.8‰) that were slightly lower than $\delta^{13}C$ values of Middle Devonian seawater (+1 to +2‰ PDB: Popp et al., 1986; Qing and Mountjoy, 1989) reflected ^{12}C-enriched CO_2 produced by organic matter oxidation related to hydrocarbon generation or thermochemical sulphate reduction.

$\delta^{18}O$ values in these dolomite deposits range widely, from -1.6 to -16.0‰ (PDB; Fig. 5a, b). Qing and Mountjoy (1994a) noted that SD and CCD had similar ranges for both $\delta^{18}O$ values (-7.0 to -16.0‰) and $\delta^{13}C$ (+1.7 to -3.8‰). In addition, SD and CCD had similar compositions at any given locality. These authors further showed that isotopic values above and below the Watt Mountain unconformity were comparable, a conclusion also corroborated from their fluid inclusion study (see below). SD and CCD evidently formed from fluids with similar $\delta^{18}O$ and $\delta^{13}C$ compositions, and precipitated throughout these Middle Devonian strata at the same time. $\delta^{18}O$ values for both SD and CCD were more negative than those of MCD and FCD (Fig. 5a, b). Qing and Mountjoy (1994a) interpreted CCD to represent limestone dolomitized during burial in which SD precipitated immediately following CCD as cements in fractures and vugs. The intimate association of SD with sulphide minerals, dissolution vugs and breccias at Pine Point led these authors to suggest the involvement of hydrothermal fluids during later burial diagenesis.

FCD described in Qing (1998a) has the highest $\delta^{18}O$ values encountered in his study, ranging from -1.6 to -3.8‰, and lowest $^{87}Sr/^{86}Sr$ ratios, which range from 0.7079 to 0.7081 (Fig. 5b, c). This phase was interpreted to represent dolomitization from Middle Devonian seawater, either at or just below the seafloor. FCD sampled close to the Pine Point orebodies (i.e. altered fine-crystalline dolomite, light blue boxes in Fig. 5) were interpreted as altered by later diagenetic fluids, explaining their lower $\delta^{18}O$ values (-6.7 to -7.9‰) and higher $^{87}Sr/^{86}Sr$ ratios (0.7082 to 0.7083). The more ^{18}O-depleted values of MCD (-3.7 to -9.4‰) and slightly higher $^{87}Sr/^{86}Sr$ ratios (0.7081to 0.7087) led Qing (1998a) to conclude that MCD precipitated either 1) from burial compaction fluids derived from Middle Devonian seawater during shallow to intermediate burial at slightly elevated temperatures (35–40°C), or 2) alternatively, shortly following deposition of the precursor sediment in the Elk Point Basin. In the latter case, the more ^{18}O-depleted values and slightly higher $^{87}Sr/^{86}Sr$ ratios were explained as having resulted from subsequent neomorphism by hydrothermal fluids during later burial diagenesis.

$^{87}Sr/^{86}Sr$ ratios of SD and CCD are largely similar, ranging from 0.7081 to 0.7121 (Fig. 5b, c). The more radiogenic values are from dolomite in the western part of Qing and Mountjoy's (1994a) study area, and reflect derivation of Sr from buried clastic sequences downdip to the west or possibly the underlying Precambrian crystalline basement. Qing's (1991) data show that the most radiogenic Sr is also associated with one of the more negative $\delta^{18}O$ values of approximately -15.5‰ (Fig. 5b).

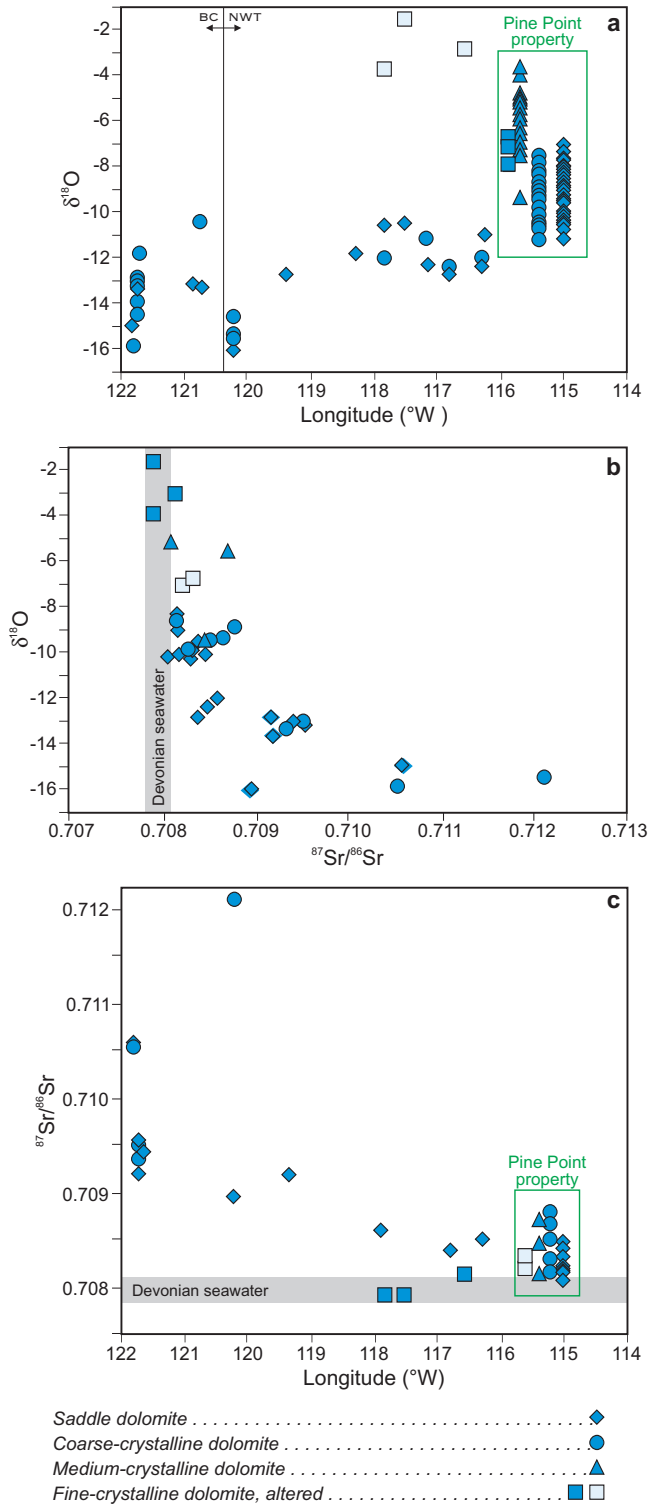

Figure 5. a. $\delta^{18}O$ (‰, PDB) vs. location for samples analyzed in Qing's (1991) study. Samples from Pine Point property are not plotted according to longitude. NWT = Northwest Territories, BC = British Columbia. **b.** $\delta^{18}O$ (‰, PDB) vs. $^{87}Sr/^{86}Sr$ for samples analyzed in Qing's (1991) study. $^{87}Sr/^{86}Sr$ for Devonian seawater is from Burke et al. (1982). Additional $\delta^{18}O$ analyses are presented in Qing (1991), but do not have corresponding strontium analyses. **c.** $^{87}Sr/^{86}Sr$ vs. location for samples analyzed in Qing's (1991) study. Samples from Pine Point Property are not plotted according to longitude. $^{87}Sr/^{86}Sr$ for Devonian seawater is from Burke et al. (1982).

Qing (1991) also reported stable carbon and oxygen isotopic analyses for late-stage, mostly post-dolomitization calcite. Both $\delta^{18}O$ and $\delta^{13}C$ values ranged widely. $\delta^{18}O$ values varied from -16.7 to –6.1‰ whereas $\delta^{13}C$ values ranged from –6.9 to +1.4‰. No co-variance was observed. Depleted $\delta^{18}O$ values were interpreted, in conjunction with the fluid inclusion homogenization temperatures of 70 to 176°C, to indicate precipitation from warm diagenetic fluids. The similar $\delta^{13}C$ values to SD and CCD indicated the input of light carbon, possibly derived from alteration of organic matter during burial, either through hydrocarbon generation or thermochemical sulphate reduction.

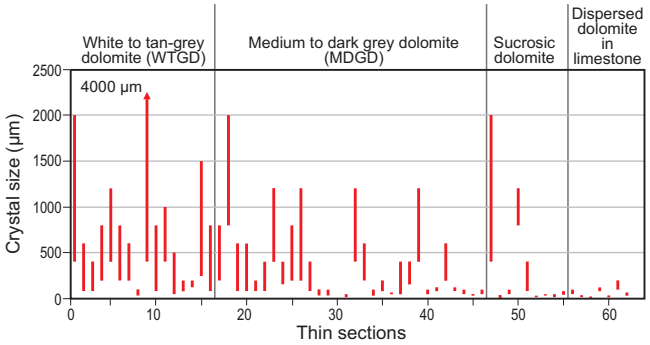

Figure 6. Range of crystal sizes (µm) of replacive dolomite in thin sections examined in this study.

Fluid inclusions

Dolomite fluid inclusion data reported by Qing and Mountjoy (1994a) are also included in Table 3. These data are derived from small (5–10 µm) two-phase aqueous fluid inclusions considered to be primary in origin because of their concentration in planes parallel to crystal growth surfaces in SD. These results coupled with $\delta^{18}O$ paleothermometry indicated dolomitizing fluids to have $\delta^{18}O_{H_2O}$ values of -1 to +5‰ SMOW, values that are 1 to 8‰ heavier than estimates for Middle Devonian seawater (-3 to -2‰ SMOW).

PETROGRAPHY: THIS STUDY

Dolomite types

We recognize five types of dolomite in these rocks: 1) saddle dolomite cement (SD), ranging mostly from 200 µm to 6 mm in size; 2) white to tan-grey replacive dolomite (WTGD), from 30 to 4000 µm; 3) medium to dark grey replacive dolomite (MDGD), ranging from 5 to 2000 µm in size; 4) sucrosic replacive dolomite, which ranges from 10 to 2000 µm in size; and 5) isolated, euhedral to anhedral dolomite crystals in limestone, typically ranging from 10 to 400 µm in size (Fig. 6). With the exception of rare, slightly potassium-ferricyanide-stained zones in several samples, all the dolomite considered in this study is nonferroan. Beyond the Pine Point property, sulphides are very rarely encountered.

The recognition of distinctive dolomite types based on crystal size, as carried out earlier by Qing (1991; Table 3), was not deemed feasible based on the cores and thin sections we examined. Our observations show that considerable variation in dolomite crystal size occurs even on a thin-section scale (Fig. 6), despite small variations in petrographic properties, such as abundance of inclusions and cathodoluminescence (discussed further below). Crystals comprising WTGD and MDGD span the range of the medium- and coarse-crystalline dolomite (MCD: 150 to 250 µm; CCD: 500 µm to 2 mm) recognized by Qing (1998a) and Qing and Mountjoy (1994a). Mosaics composed of FCD, with crystals ranging from 5 to 25 µm in size are also encountered in these rocks, although such fine mosaics are reported to be more typical of back-barrier facies of the Muskeg Formation (Qing, 1998a).

The typical Presqu'ile fabric, including nonbrecciated and brecciated, is dominated by varying proportions of SD and MDGD, and to a lesser extent, WTGD (Fig. 7a, b, c). Distinctive zebraic texture composed of discontinuous bands of SD and MDGD also occur (Fig. 7d). Presqu'ile dolomite fabric is widespread throughout the study area but most abundant in the Pine Point property region. Presqu'ile fabric also occurs throughout the stratigraphic succession, but is most extensively developed in the Slave Point, Sulphur Point and Pine Point formations. More rarely, it occurs patchily in the Muskeg and Keg River formations. Some core shows incipient development of the Presqu'ile fabric, where the surrounding dolomite is more fine crystalline and may retain vestiges of the original depositional fabric.

Cement and replacive dolomite mosaics, with the exception of sucrosic dolomite, form mostly nonplanar to planar-s textures (Sibley and Gregg, 1987). SD is characteristically white, displays the typical curved crystal faces where crystals line pores, and has a pronounced undulatory extinction when viewed with crossed polars. SD occurs in vugs, fractures and inter-breccia clast spaces as overgrowths on surrounding replacive dolomite. SD rarely occurs within vugs in limestone.

Replacive dolomite and SD are typically fluid inclusion-rich with the crystal interiors being usually more inclusion-rich than the rims (Fig. 8a, c, e), although some crystals have relatively clear cores and inclusion-rich rims. Many mosaics are composed of crystals that have rims, or sometimes irregular domains within crystals, that are stained a light to medium brown in transmitted light, and are relatively inclusion-free (Fig. 8e).

Replacive dolomite in these rocks, specifically WTGD, MDGD and sucrosic (planar-e texture) dolomite, are very similar petrographically. The difference between WTGD and MDGD results from the slightly greater amount of intercrystalline porosity in the latter, and the greater abundance of a dark intercrystalline material tentatively identified as bitumen. These two types of replacive dolomite, which also

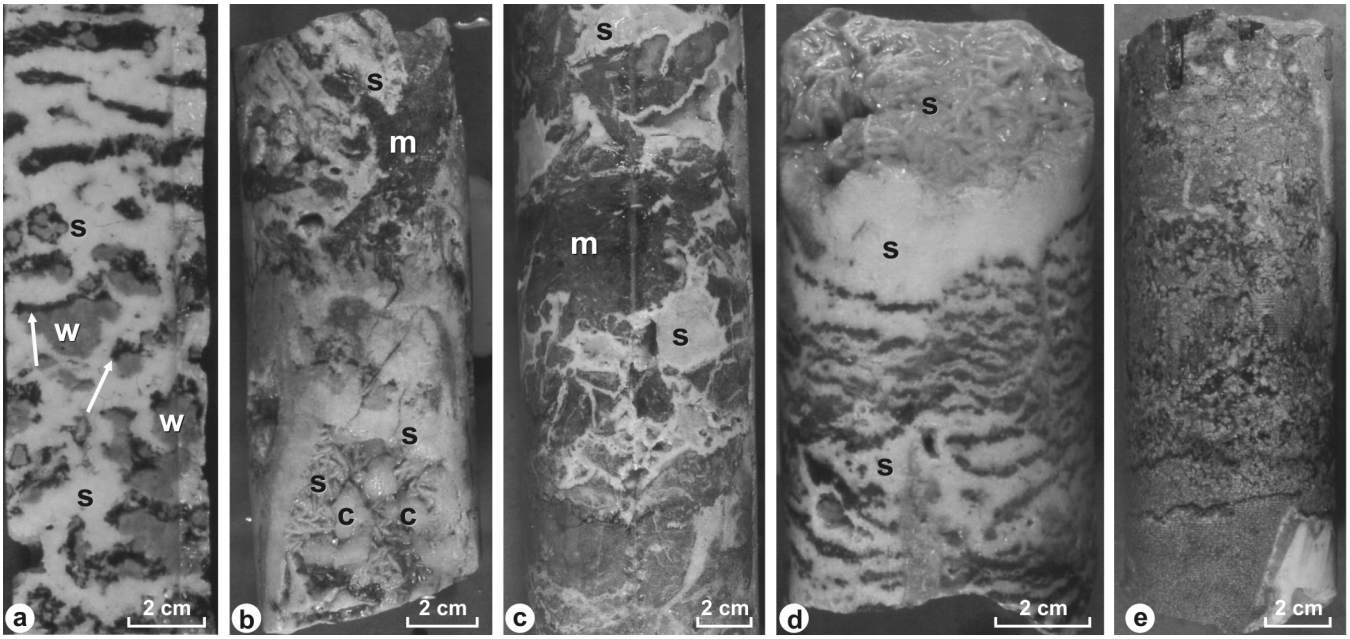

Figure 7. Core photographs. **a.** Presqu'ile dolomite fabric, showing geopetal arrangement of MDGD (white arrows) on WTGD (w) surrounded by white SD cement (s). General Crude Ranvik Reef Creek G-15, 280.4 m depth, Sulphur Point Formation. **b.** Breccia composed of MDGD (m) in Presqu'ile dolomite. Saddle dolomite cement (s) filling and lining pores is followed by late-stage, coarse-crystalline calcite cement (c). NWT Heart Lake #1 F-29, 490.1 m depth, Pine Point Formation. A photomicrograph of the saddle dolomite cement and calcite is shown in Figure 8a. **c.** Breccia in Presqu'ile dolomite. Breccia clasts are MDGD (m) dolomite cemented by saddle dolomite (s). Placid Wood West Tathlina K-48, 942.1 m depth, Pine Point Formation. **d.** Zebraic texture in Presqu'ile dolomite. Discontinuous layers of MDGD are surrounded by white saddle dolomite cement (s). NWT Heart Lake #1 F-29, 492.6 m depth, Pine Point Formation. **e.** Rare example of coarse sucrosic replacement dolomite, with most crystals from 400 µm to 2 mm in size. Horn River et al. Hay River B-52, 171.1 m depth, Watt Mountain Formation. A photomicrograph of this fabric is shown in Figure 8c.

have undulatory extinction, sometimes form a kind of "snow on roof" fabric (Fig. 7a), which is commonly seen with sulphides in the Pine Point orebody (Leach and Sangster, 1993), whereby the more porous, darker coloured MDGD overlies WTGD on the upper surfaces of partly replaced dolomitized breccia fragments.

Well-developed sucrosic fabrics are comparatively rare, and tend to be more fine crystalline, although some coarse-crystalline examples, with crystals up to 1 mm or more, locally occur (Fig. 7e).

Cathodoluminescence

The cathodoluminescence characteristics of these dolomite samples are more complicated than indicated in earlier studies. Qing (1991) indicated that SD displays deeper red cores and lighter red rims (not uniform bright orange cathodoluminescence as described in Qing and Mountjoy, 1994a), and that some SD had zoning but the zoning could not be correlated regionally. CCD had a uniform dull red luminescence, whereas MCD was characterized by red/orange cathodoluminescence with bright orange blotches along some crystal boundaries.

Thin sections examined in this study reveal that the cloudy, inclusion-rich portions of most SD and the matrix dolomite crystals display the typical "blotchy" luminescence described from numerous other studies of dolomite (Fig. 8b, d, f). This texture consists of an even mixture of micrometre to submicrometre irregular domains of bright red luminescence and usually dull or weak red luminescence. The correspondence of these blotchy domains with the inclusion-rich portions of crystals suggests that at least some of this texture may be the result of irregular pits on the surfaces of the polished crystals or it could also be compositional and the result of recrystallization (e.g. Dorobek et al., 1993). Saddle dolomite within vuggy and fracture pores in limestone is mostly nonluminescent.

In contrast, the relatively inclusion-free rims of crystals and those relatively inclusion-free parts of crystals having the irregular brown stain are characteristically dull or weak red luminescent, or more rarely are nonluminescent (Fig. 8b, d, f). These rims also commonly show subtle, fine-scale concentric compositional zoning. Crystals within a sample display the same succession of fine-scale zones, but correlation of zones between samples is not possible.

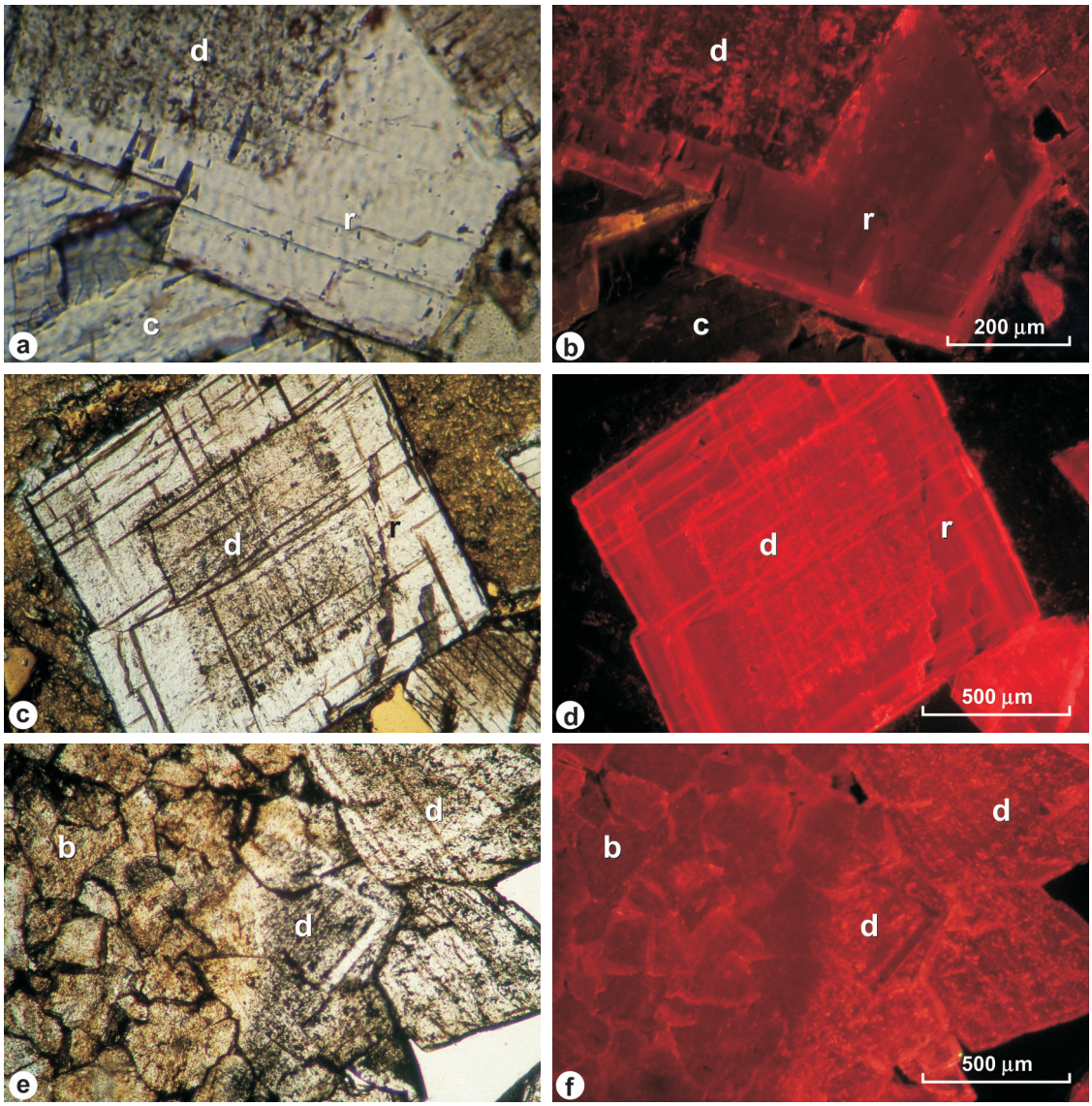

Figure 8. Paired plane-light and cathodoluminescence photomicrographs. **a, b.** View of saddle dolomite cement with cloudy, inclusion-rich core (d) and relatively clear, inclusion-poor rim (r). Note characteristic blotchy luminescence of the core area compared to the dull to bright red-zoned rim. Brown luminescent late-stage calcite (c) fills remaining porosity. Thin section is from Presqu'ile fabric seen in Figure 7b. Thin section C-421082, NWT Heart Lake #1 F-29, 490.1 m depth, Pine Point Formation. **c, d.** View of coarse-crystalline sucrosic dolomite showing blotchy luminescent, inclusion-rich core (d) and relatively inclusion-poor rim (r) composed of alternating zones of dull and bright red luminescent dolomite. Thin section is from sucrosic dolomite seen in Figure 7e. Thin section C-421066, Horn River et al. Hay River B-52, 171.1 m depth, Watt Mountain Formation. **e, f.** MDGD mosaic showing crystals (b) with brown stain and dull luminescence overlain by blotchy luminescent, inclusion-rich dolomite cement (d). Note the dull luminescent, inclusion-free zone in the cement. Thin section C-421133, borehole 2829 on Pine Point property, 105.5 m depth, Pine Point Formation.

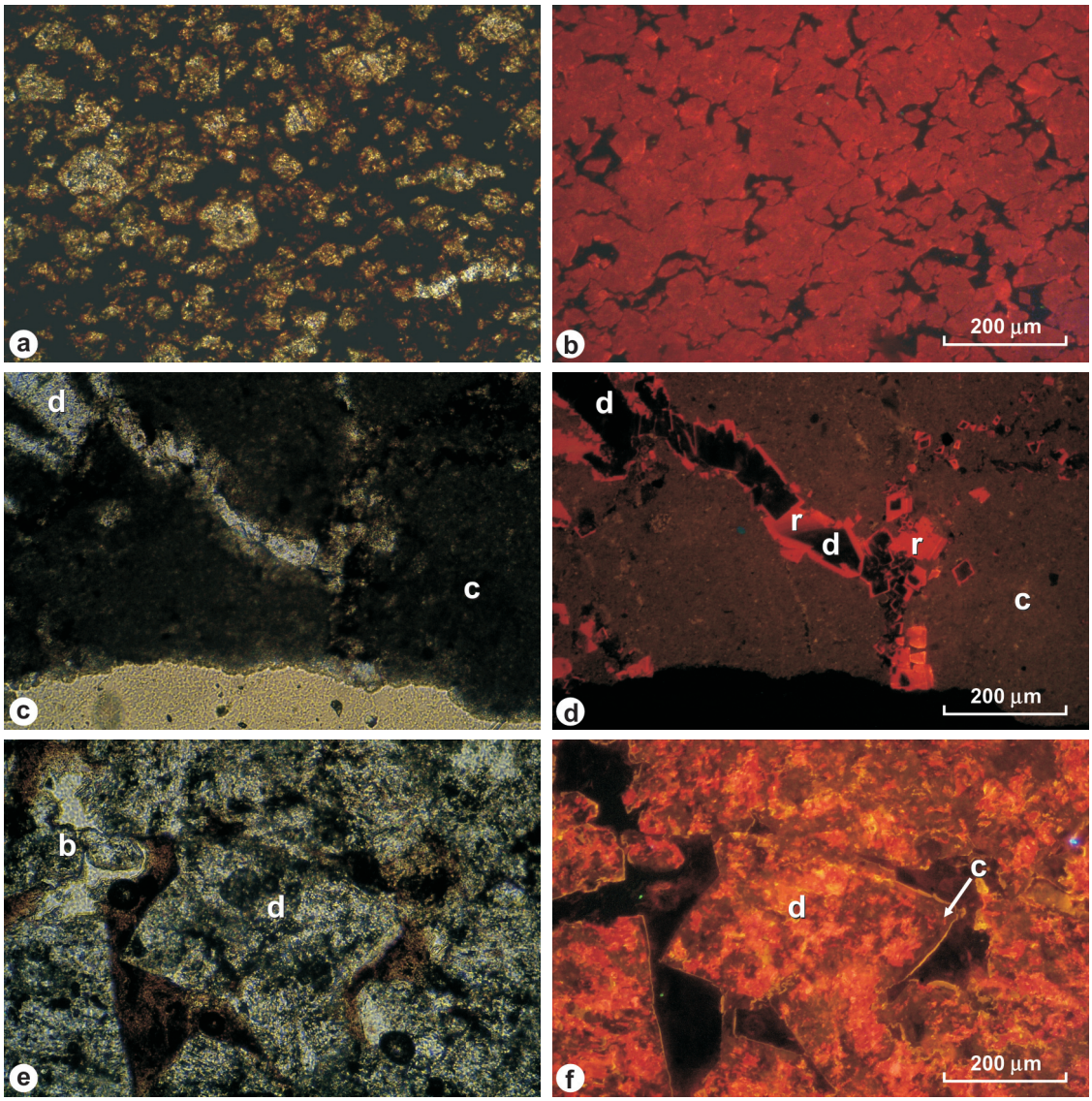

Figure 9. Paired plane-light and cathodoluminescence photomicrographs. **a, b.** MDGD mosaic composed of dull luminescent, relatively fine-crystalline (80 to 120 µm) dolomite. Thin section C-421134, borehole 2829 on Pine Point property, 130.9 m depth, Pine Point Formation. **c, d.** Dispersed dolomite in micritic, brown luminescent limestone (c) has non-luminescent (dark) cores (d) and bright red rims (r). Thin section C-421136, borehole 3293 on Pine Point property, 18.7 m depth, Slave Point Formation. **e, f.** MDGD mosaic composed of blotchy luminescent dolomite (d) that is partly replaced by brown luminescent calcite (dedolomite) (c). Thin section C-421116, borehole 2822 on Pine Point property, 100.3 m depth, Sulphur Point Formation.

The more fine crystalline matrix dolomite which preserves original depositional fabric tends to be more evenly dull luminescent overall (Fig. 9a, b), although coarser crystals do show that fine-scale zoning with medium to bright red zones may be present. Dolomite crystals in partially dolomitized limestone may have nonluminescent cores and bright red rims (Fig. 9c, d).

Dolomite is generally overlain in pores in which it fills incompletely, by a late-stage weak yellow to brown, luminescent, nonferroan, late-stage calcite, which may show concentric, and sometimes also pronounced sectoral zoning. In most cases dolomite appears relatively unaltered, but rarely, some dolomite is replaced by nonferroan, brown-luminescent calcite (dedolomite – Fig. 9e, f), indicating that at least localized alteration occurred either prior to or during precipitation of the late-stage pore-filling calcite.

STABLE CARBON AND OXYGEN ISOTOPES

Dolomite

Representative dolomite samples, with the exception of dispersed dolomite in limestone, were analyzed for $\delta^{13}C$ and $\delta^{18}O$ values (Fig. 10; Table 2). Overall, the distribution of values shows a limited range of $\delta^{13}C$ values, mostly between -1 and +3‰, and a wide range of $\delta^{18}O$ values from -13 to -1‰. There is no obvious co-variance between $\delta^{13}C$ and $\delta^{18}O$ values.

SD (n = 24) $\delta^{18}O$ values range from -13.0 to -7.2‰. $\delta^{13}C$ values are mostly slightly positive, ranging from -0.9 to +2.7‰. The one exceptional sample with a $\delta^{13}C$ value of +11.8‰ otherwise displays typical petrographic characteristics and $\delta^{18}O$ value (-8.0‰).

WTGD $\delta^{18}O$ values range mostly between -9.1 and -12.4‰, whereas MDGD ranges from -7.0 to -13.2‰. Both types of dolomite also have more positive $\delta^{18}O$ values, up to -4.1‰ for WTGD and -0.8‰ for MDGD, than SD. The $\delta^{13}C$ values for WTGD range from -0.9 to +3.2‰ and for MDGD from -0.8 to 2.7‰. The close similarity of $\delta^{13}C$ and $\delta^{18}O$ values for WTGD and MDGD confirm what the petrography suggests – that these two types of dolomite are the same phase, and their differences, principally colour in core sample, reflect the higher intercrystalline porosity of MDGD and inclusion of dark material (bitumen?) in these spaces. Only three samples of sucrosic dolomite were analyzed. $\delta^{18}O$ values range from -12.7 to -8.6‰, whereas $\delta^{13}C$ values range from +0.5 to +2.4‰.

A graph of dolomite $\delta^{18}O$ value vs. maximum dolomite crystal size shows no obvious relationship (Fig. 11) between these parameters, unlike other examples of recrystallized burial dolomite in the literature, where correlated $\delta^{18}O$ value decreases and crystal size increases suggested progressive recrystallization (e.g. Mazzullo, 1992). For example, five samples with the highest $\delta^{18}O$ values (> approx. -4‰) in this study are dominated by mosaics composed of crystals less than 500 µm in size. Samples dominated by fine-crystalline mosaics also have some of the most negative $\delta^{18}O$ values.

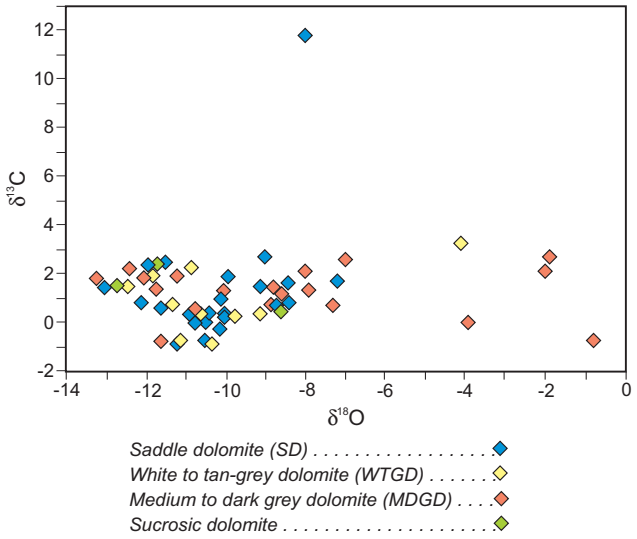

Figure 10. $\delta^{13}C$ (‰, PDB) vs. $\delta^{18}O$ (‰, PDB) for all dolomite samples analyzed in this study.

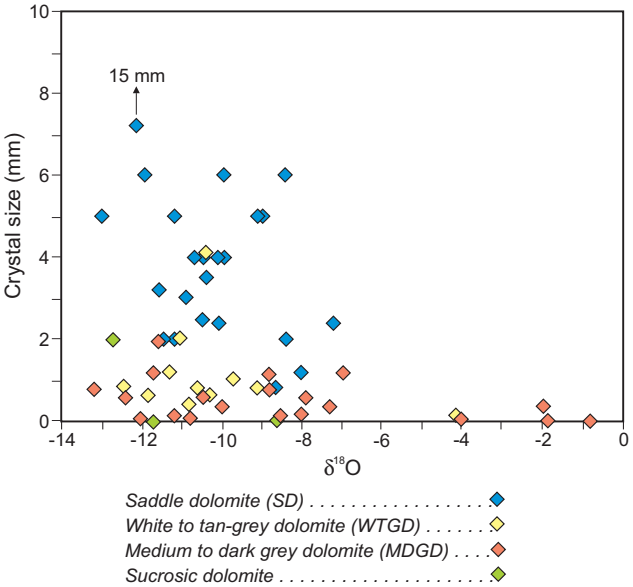

Figure 11. $\delta^{18}O$ (‰, PDB) vs. maximum crystal size (mm) for dolomite samples analyzed in this study.

Interpretation

The results of this study, even though restricted to the southern NWT and with no data from NEBC, do not support the existence of the regional trend described in Qing and Mountjoy (1994a) where $\delta^{18}O$ values of SD decreased westward from an average of approximately -9.0‰ at Pine Point to approximately -14‰ in NEBC (Fig. 12). The $\delta^{13}C$ and $\delta^{18}O$ values of CCD, as reported in Qing (1991), because they are so similar to the SD values, also show this westward-decreasing trend. Rather, our study shows that $\delta^{18}O$ of SD, as well as any of the replacive dolomite across our study area, display similar values to those encountered at the Pine Point property (Fig. 13).

The wide spread of $\delta^{18}O$ values at each location combined with the lack of a geographic trend may support an interpretation of local convective overturn of dolomitizing fluids, rather than an interpretation involving regional fluid migration (Morrow, 1998). Site-specific variations in $\delta^{18}O$ values could be explained by controls such as temporal, possibly episodic, variations in basal heat flow during convective overturn or variations in the degree of recrystallization (i.e.

differing water-rock ratios), perhaps controlled by fluid-flow pathways as a function of porosity and permeability (e.g. Nielsen et al., 1994; Coniglio et al., 2003).

Calcite

Late-stage, post-dolomitization calcite samples (n = 8) have widely ranging $\delta^{18}O$ values from -15.3 to -4.9‰ and $\delta^{13}C$ values from -17.4 to +3‰ (Fig. 14). One sample of fibrous marine calcite has a $\delta^{18}O$ value of -4.9‰ and a $\delta^{13}C$ value of +2.2‰. The few data that exist suggest a possible weak covariance between $\delta^{13}C$ and $\delta^{18}O$ values.

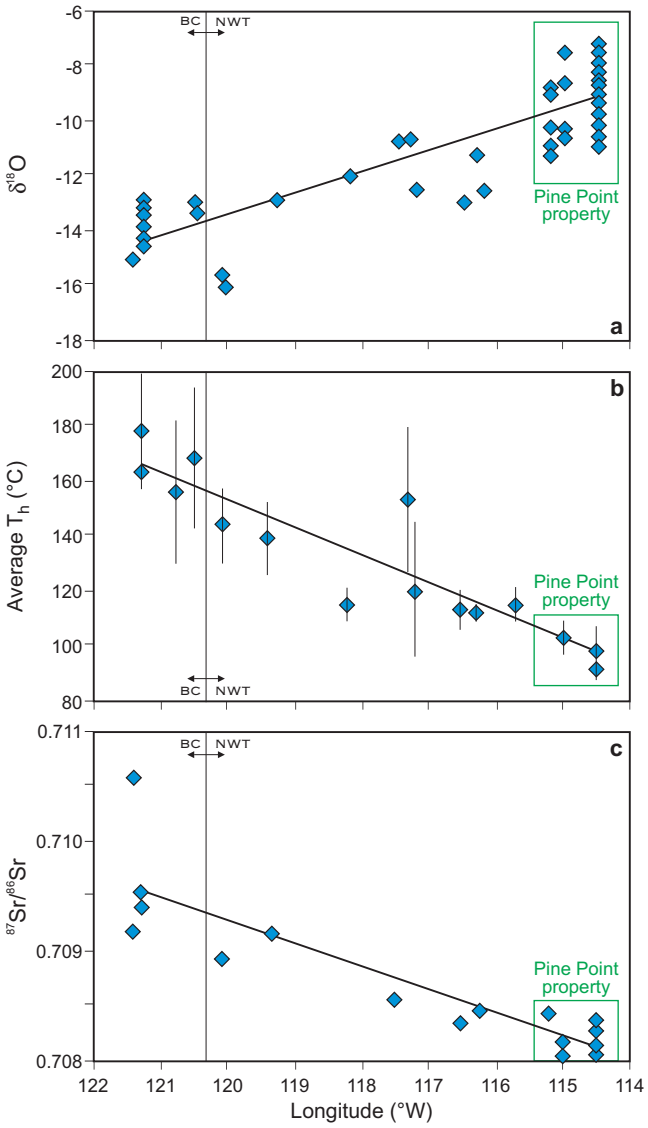

Figure 12. Cross plots of **a.** $\delta^{18}O$ (‰, PDB), **b.** T_h (°C), and **c.** $^{87}Sr/^{86}Sr$ of saddle dolomite cements vs. longitude. Diagram is *modified from* Qing and Mountjoy (1994a).

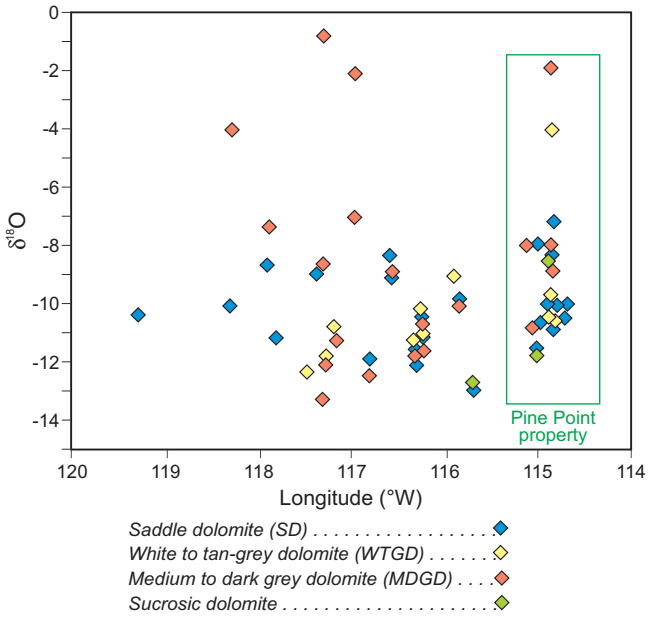

Figure 13. $\delta^{18}O$ (‰, PDB) vs. longitude for all dolomite samples analyzed in this study. Longitude information for Pine Point property is not accurate.

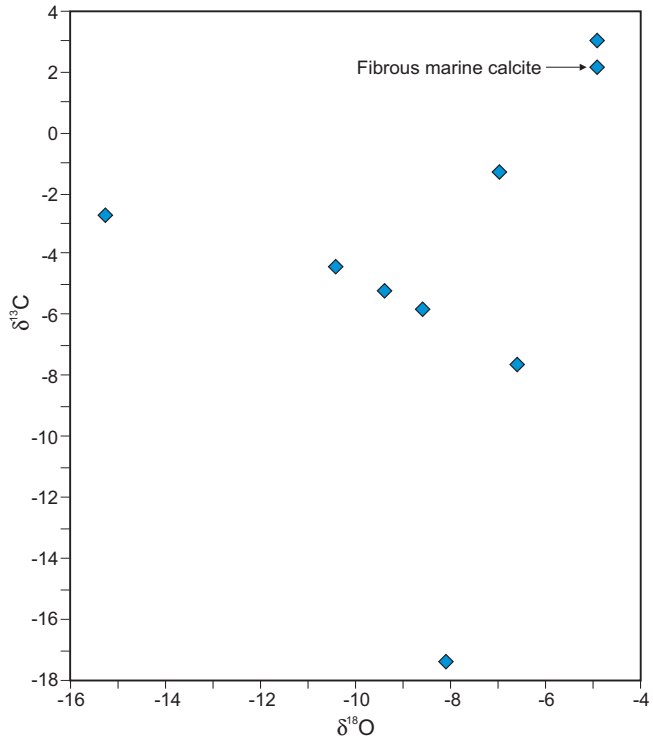

Figure 14. $\delta^{13}C$ (‰, PDB) vs. $\delta^{18}O$ (‰, PDB) for all calcite samples analyzed in this study.

Interpretation

Oxygen isotopic compositions suggest burial is a dominant influence, although fluid inclusion evidence (see below) suggests that fluids were not as saline as for dolomite. Rather, fluid inclusions suggest that some admixture of meteoric fluids with subsurface brines during precipitation of blocky calcite occurred. This is consistent with the petrographically "late" aspect of coarse-crystalline calcite at Pine Point. Strong negative $\delta^{13}C$ values of calcite suggest involvement of organic degradation reactions (e.g. thermochemical sulphate reduction, methane oxidation, decarboxylation).

RADIOGENIC STRONTIUM ISOTOPES

Dolomite

$^{87}Sr/^{86}Sr$ values of the different dolomites recognized in this study overlap and are all more radiogenic than the upper limit of 0.7081 for Middle Devonian seawater (Fig. 15; Table 2; Burke et al., 1982). Saddle dolomite $^{87}Sr/^{86}Sr$ values range from 0.70817 to 0.70909, and WTGD values range from 0.70841 to 0.70857. MDGD values range mostly from 0.70816 to 0.70932, although one value of 0.71119 is considerably more radiogenic. A single sample of sucrosic dolomite has a $^{87}Sr/^{86}Sr$ value of 0.70852. There is no discernible trend between dolomite $\delta^{18}O$ and $^{87}Sr/^{86}Sr$ values in these rocks (Fig. 15). In addition, as with $\delta^{18}O$ values, there is no relationship between maximum dolomite crystal size in a sample and its $^{87}Sr/^{86}Sr$ value (Fig. 16). Lastly, dolomite $^{87}Sr/^{86}Sr$ values in the current study do not show any trend related to their geographic distribution (Fig. 17).

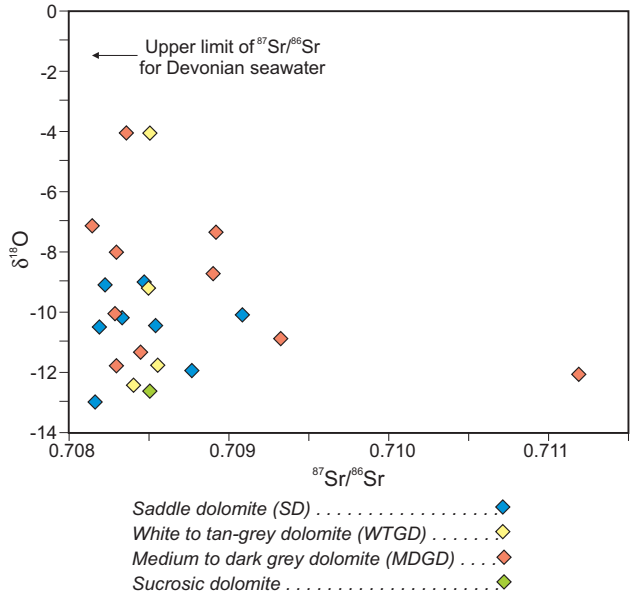

Figure 15. $\delta^{18}O$ (‰, PDB) vs. $^{87}Sr/^{86}Sr$ for all dolomite samples analyzed in this study. The upper limit of $^{87}Sr/^{86}Sr$ for Devonian seawater is from Burke et al. (1982).

Interpretation

$^{87}Sr/^{86}Sr$ values tend to cluster between 0.07080 and 0.07090, or just above the upper value for Middle Devonian seawater. $^{87}Sr/^{86}Sr$ values of dolomite analyzed in this study are comparable to values reported in Qing (1991), which range from 0.7079 to 0.7121. Unlike most late-stage dolomite in the Western Canada Sedimentary Basin, which shows significant input of radiogenic strontium (>0.7100 up to 0.7151), those at Pine Point and in the subsurface to the west are considerably less radiogenic, leading Mountjoy et al. (1992) to suggest the involvement of recycled Devonian

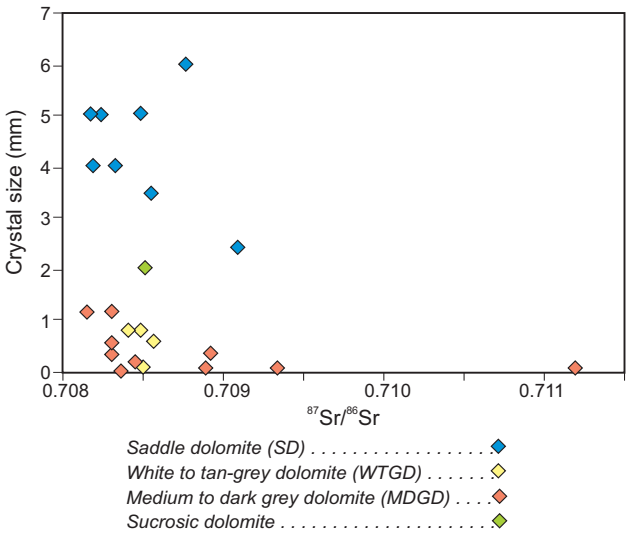

Figure 16. $^{87}Sr/^{86}Sr$ vs. maximum crystal size (mm) for all dolomite samples analyzed in this study.

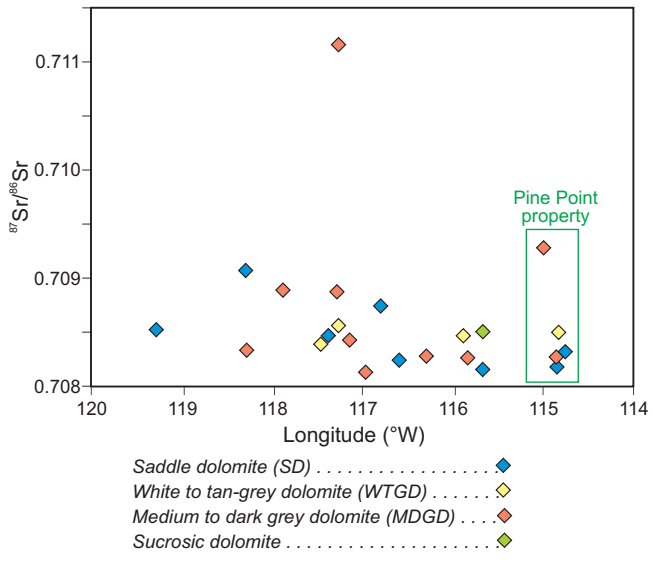

Figure 17. $^{87}Sr/^{86}Sr$ vs. longitude for all dolomite samples analyzed in this study. Longitude information for Pine Point property is not accurate.

strontium, perhaps from pressure solution of other Devonian carbonate. The ultimate source of radiogenic strontium could have resulted from reaction of brines with feldspars or from rubidium in clay minerals within or beneath the Phanerozoic strata.

Calcite

Only two samples of late-stage calcite were analyzed in this study, yielding $^{87}Sr/^{86}Sr$ values of 0.71337 and 0.71551. These values are considerably more radiogenic than the dolomite values, a characteristic that was also noted by Qing (1991) in the late-stage calcites (n = 11) he analyzed, where $^{87}Sr/^{86}Sr$ values ranged from 0.70850 to 0.71613.

Interpretation

The fluids that precipitated the calcite reflect more extensive rock-water interactions than those preceding fluids that precipitated the dolomite. Mountjoy et al. (1992) considered brines that precipitated late-stage calcite on a regional scale to be the most ^{87}Sr-enriched fluids in the Western Canada Sedimentary Basin. The source for such high levels of radiogenic strontium remains speculative. Mountjoy et al. (1992) suggested that the association of many of these late-stage calcites with anhydrite indicates precipitation from basinal brines. These authors also suggested the possibility of mixing with younger meteoric waters from the Shield, which, if modern examples are typical, can be strongly radiogenic (e.g. McNutt et al., 1990). The lower salinity of primary fluid inclusions in late-stage calcites (see below) lends some support to this explanation, although the low Sr concentrations of most meteoric waters (e.g. McNutt et al., 1990) suggest that fluids that resulted from mixing would have probably had salinities much lower than those measured in this study (discussed further below).

FLUID INCLUSION ANALYSIS

Fluid inclusion data are reported from four samples containing varying amounts of saddle dolomite and late-stage calcite (Table 4). The fluid inclusion study was complicated by the lack of suitable assemblages in finer crystalline WTGD and MDGD, the unknown origin of many fluid inclusion assemblages, which did not allow the populations to be related to paragenesis of the samples, and that some inclusions in populations began to stretch and do not yield representative homogenization temperatures. Therefore, the majority of analyses were performed on two-phase aqueous and petroleum inclusions from SD and late-stage calcite.

Paragenetically, primary two-phase aqueous and high-maturity petroleum inclusions in SD were overgrown by late-stage calcite that contained primary aqueous inclusions. Both SD and late-stage calcite were subsequently truncated by secondary low-maturity petroleum and aqueous inclusions.

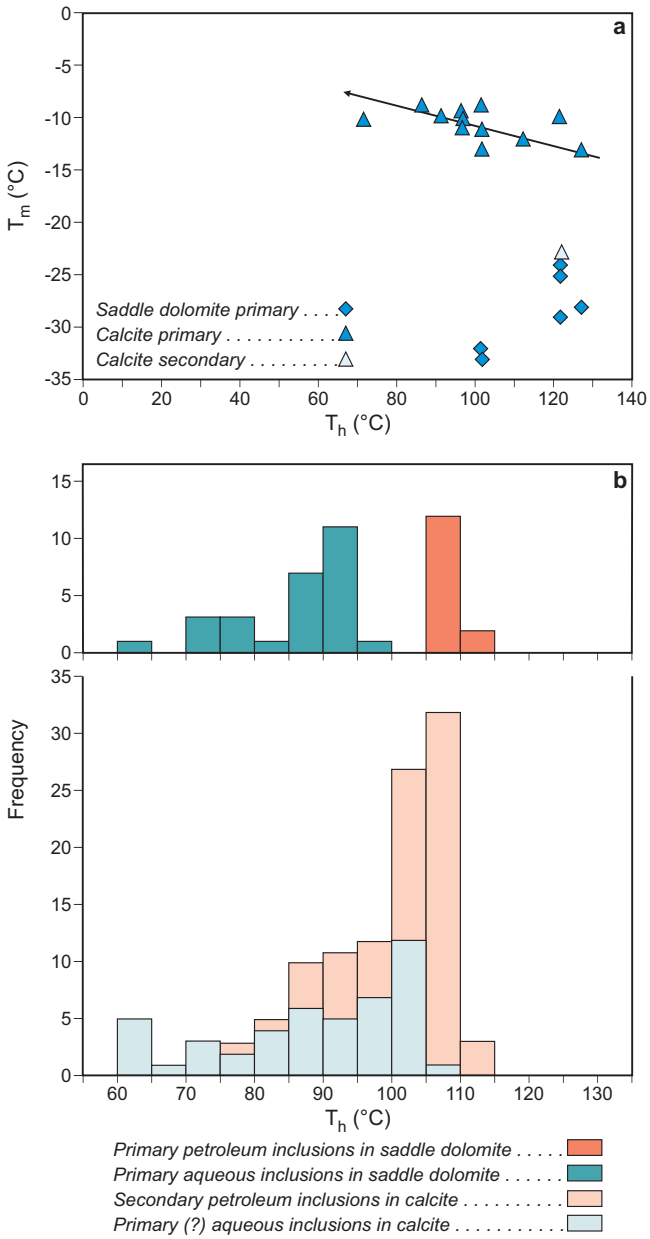

Figure 18. a. Plot of T_h (°C) vs. T_m (°C) for individual inclusions in saddle dolomite and late-stage calcite (Table 4). Data from dolomite and calcite are clearly separated in T_h vs. T_m space and there may be some evidence for fluid mixing (arrow), possibly with less saline meteoric fluids, during precipitation of calcite. **b.** Fluid inclusion homogenization temperatures for SD and late-stage calcite from sample C-421115. Primary petroleum inclusions (100–110°C) in SD were trapped with aqueous inclusions that recorded broader lower temperatures (60–95°C). Late calcite trapped primary two-phase inclusions (60–110°C) and were cut by later secondary petroleum inclusions at 75–115°C.

Table 4. Summarized individual fluid inclusion data

Sample number	Mineral host	T_h (°C)	T_m (°C)	Eq. NaCl %	Type	T_e (°C)	System
C-421076	dolomite	125	-28	27.4	Primary	<-60	NaCl-$CaCl_2$
C-421076	dolomite	120	-29	28.0	Primary	<-65	NaCl-$CaCl_2$
C-421076	dolomite	120	-25	25.6	Primary	<-65	NaCl-$CaCl_2$
C-421076	dolomite	120	-24	25.0	Primary	<-60	NaCl-$CaCl_2$
C-421083	dolomite	100	-32	30.0	Primary	<-50	NaCl-$CaCl_2$
C-421083	dolomite	100	-33	30.6	Primary	~ - 60	NaCl-$CaCl_2$
C-421115	dolomite	85	-	-	Primary	<-80	NaCl-$CaCl_2$
C-421083	calcite	95	-11	15.0	Primary	<-35	NaCl
C-421083	calcite	70	-10.2	14.1	Primary	<-35	NaCl
C-421083	calcite	95	-10	13.9	Primary	<-45	NaCl
C-421083	calcite	100	-13	16.9	Primary	<-55	NaCl
C-421083	calcite	110	-12	16.0	Primary	<-50	NaCl
C-421083	calcite	100	-11	15.0	Primary	<-35	NaCl
C-421101	calcite	125	-13	16.9	Primary	-40	NaCl
C-421101	calcite	120	-23	24.3	Secondary	-40	NaCl
C-421101	calcite	95	-9.6	13.5	Primary	-40	NaCl
C-421115	calcite	120	-10	13.9	Primary	<-52	NaCl
C-421115	calcite	85	-8.8	12.6	Primary	<-45	NaCl
C-421115	calcite	90	-10	13.9	Primary	-48.5	NaCl
C-421115	calcite	100	-8.8	12.6	Primary	-45	NaCl

Homogenization temperatures of primary aqueous inclusions in SD range from 70 to 135°C, although within individual samples, the range is considerably less (e.g. Fig. 18a, b). Similarly, homogenization temperatures of rare secondary aqueous inclusions in SD range from 120 to 150°C. Trapped fluids are NaCl-$CaCl_2$ brines, with salinities calculated at 25 to approximately 30 wt % NaCl equivalent (Table 4). High-maturity, green to greenish white fluorescent (see Stasiuk and Snowdon, 1997) primary petroleum inclusions occur along interior crystal growth zones in SD and homogenized between 100 to 110°C (Fig. 18b), and 120 to 125°C (this range was recorded in a separate sample; not shown in Fig. 18b).

Primary aqueous fluid inclusions in late-stage calcite in all samples generally have lower homogenization temperatures between 60 to 125°C although the range significantly overlaps the SD data. For example, in sample C-421115, late-stage calcite trapped primary two-phase aqueous inclusions with homogenization temperatures ranging from 60 to 110°C (Fig. 18b). These aqueous inclusions were then cut by later secondary petroleum inclusions with homogenization temperatures from 75 to 115 °C (Fig. 18b). Salinities are significantly lower than SD and range from <13 to 17 wt % NaCl equivalent, were derived from NaCl fluids, and suggest some mixing with less saline fluids (Fig. 18a; Table 4).

Late petroleum inclusions (plus associated aqueous inclusions) are common in some samples, are of secondary origin, and homogenized between 60 to 130°C. Rare primary petroleum inclusions (single sample) are similar to the secondary inclusions in that sample, and have homogenization temperatures ranging from 95 to 105°C.

The fluid inclusion data indicate that 1) SD has consistently high salinities, therefore fluid mixing was not significant as a precipitation mechanism during dolomitization; 2) primary inclusions in late-stage calcite have lower salinities and do suggest some mixing with possible meteoric fluids (Fig. 18a); and 3) homogenization temperatures may be unreliable as they range broadly. As pointed out by Morrow (1998), the high salinity of primary fluid inclusions in these carbonate deposits implies that dolomitization and precipitation of late-stage calcite were unlikely to have been influenced by freshwater recharge during regional groundwater flow associated with topographic recharge in highlands to the west.

Comparison with previous fluid inclusion data from carbonate samples

Qing and Mountjoy (1994a) reported T_h of primary aqueous fluid inclusions in saddle dolomite to range from 92 to 178°C, which is slightly higher than values determined in this study. Salinities presented by Qing and Mountjoy (1994a) range from 10 to 28 wt % NaCl equivalent, which again is broader than the range observed in this study. This broader range could be explained by precipitation of SD from variable salinity fluids, which is not consistent with our data, or, more likely, by the refilling of original primary inclusions with later, lower salinity fluids. The upper end of this range is similar to salinities determined in SD whereas the lower end of this range is similar to salinities determined from late-stage calcite in this study. Fluids were determined by Qing and Mountjoy (1994a) to be dominantly NaCl and $CaCl_2$ fluids with subordinate KCl and $MgCl_2$.

Qing and Mountjoy (1994a) also reported fluid inclusion analyses from late-stage calcite and derived salinities of 6 to 19 wt % NaCl equivalent, which indicated precipitation from slightly less saline fluids than saddle dolomite from the same location. This relationship is generally verified in this study (Fig. 18a), and confirmed in the one sample that yielded both T_h and T_m data for dolomite and calcite (C-421083 in Table 4). Qing's (1991) calcite T_h values were similar to the T_h values of SD, and they also increased westward along the Presqu'ile barrier with increasing burial depth, although T_h of calcite was approximately 10°C lower than T_h of SD in the same locations.

DOLOMITIZATION MECHANISM

Qing and Mountjoy's (1994a) paleohydrological model

Qing and Mountjoy (1994a) based their paleohydrological model on the geographic distribution of dolomite $\delta^{18}O$ values, $^{87}Sr/^{86}Sr$ ratios, and fluid inclusion homogenization temperatures (Fig. 12). Note that Figure 5 in the current report includes all of Qing's (1991) dolomite isotope data, not just from SD as shown in Figure 12. From the Pine Point property westward into the subsurface of NWT and NEBC, $\delta^{18}O$ values of SD decrease from an average of approximately -9.0‰ at Pine Point to approximately -14‰ in NEBC, the result of increasing temperatures westward (Fig. 12a). Primary fluid inclusion average T_h also gradually increases with depth and downdip from Pine Point to NEBC from 92 to 178°C (Fig. 12b). $^{87}Sr/^{86}Sr$ ratios gradually increase westward, from an average of 0.7083 for SD at Pine Point, which is slightly more radiogenic than Middle Devonian seawater, to an average of 0.7095 in NEBC (Fig. 12c). These trends were interpreted as reflecting a basin-scale, eastward updip migration of hot, radiogenic fluids driven by tectonic compression, sedimentary loading and uplift of the western part of the Western Canada Sedimentary Basin. Dolomitization during this fluid flow event was probably multistaged, with groundwater driven by a combination of topographic recharge and tectonic compaction during either the Cretaceous–Tertiary Laramide Orogeny (probably the main phase) or possibly the earlier Antler Orogeny (Devonian–Carboniferous) (Morrow, 1998).

Qing and Mountjoy (1994a) envisaged the Presqu'ile barrier to have focused this flow of basinal fluids from deeply buried rocks, thus explaining the discrepancy between the T_h of SD primary fluid inclusions and reconstructed maximum burial temperatures. As fluids moved updip, they cooled. The eastward decrease in $^{87}Sr/^{86}Sr$ ratios indicate that fluids derived from downdip clastic sequences or the underlying Precambrian basement became less radiogenic as they travelled eastward and 1) were diluted by less radiogenic formation waters at shallower depths in the basin; 2) incorporated less radiogenic Sr from nonradiogenic Middle Devonian limestone; or 3) mixed with fluids having a different source (Mountjoy et al., 1992).

Reassessment in light of current data

Recent work by Morrow (1998) on hydrothermal convection models suggested that long-lived thermal convection flow systems are capable of recycling dolomitizing solutions through rock masses, especially if overlying seawater-derived solutions are continually added to the convection cell. In contrast, topographic recharge was considered to be an insufficient mechanism for predicting the uniform regional trends of dolomite precipitational temperatures and the high fluid inclusion salinities that are commonly observed in hydrothermal dolomites. Furthermore, tectonic compaction required unrealistic levels of fluid focusing to explain T_h of primary fluid inclusions in hydrothermal dolomite. Both topographic recharge and tectonic compaction were considered to be unlikely flow mechanisms to explain the extensive amounts of dolomite cement observed, based on the limited supply of solute left in the system after flushing of the solutes, thus incapacitating the formation of dolomite.

An alternative explanation for the progressive westward increase in dolomite fluid inclusion T_h as observed by Qing and Mountjoy (1994a) was offered by Morrow (1998), who suggested that the hotter paleotemperatures recorded in the western regions were a function of deeper convective circulation due to greater depth to relatively impermeable Precambrian basement in late Paleozoic time. This also explains the westward-decreasing trend in $\delta^{18}O$ values reported in Qing and Mountjoy (1994), where $\delta^{18}O$ values pass from approximately -9.0‰ at Pine Point to approximately -14‰ in NEBC.

As discussed above, newly acquired $\delta^{13}C$ and $\delta^{18}O$ values, $^{87}Sr/^{86}Sr$ values and thermometric data from fluid inclusions in this study are similar to those data obtained in Qing's (1991) study. However, our data, particularly $\delta^{18}O$ and $^{87}Sr/^{86}Sr$ values, do not show spatial trends that support Qing

and Mountjoy's (1994a) paleohydrological model for the Middle Devonian Presqu'ile barrier. This is particularly perplexing, as many of the same wells were sampled in both studies.

The blotchy cathodoluminescence seen in much of the dolomite in this study may indicate that recrystallization of the dolomite occurred during its diagenetic history, similar to that described in numerous other studies (e.g. Mazzullo, 1992; Machel, 1997). Moreover, from the expanded $\delta^{18}O$ and $^{87}Sr/^{86}Sr$ data set now available for the study area, we suggest that the spread in these values and the lack of a clear geographic trend, more realistically reflect the great variability in these parameters on a local, even borehole scale. A similar argument was put forward by Coniglio et al. (2003) to explain dolomite characterized by relatively uniform petrographic characteristics, but varying geochemistry. These authors suggested that recrystallization during progressive burial was not a uniform process, but was controlled on macro- to micro-scales by precursor rock textures, including porosity and permeability as it ultimately influenced the extent of fluid-rock interaction.

The lack of regional trends in these data is not surprising if the thermal convection model described in Morrow (1998) is applicable. The prominent, northeast-trending, mostly extensional faults in the study area (Morrow et al., 2006) and the karstic pore-system that developed in the Presqu'ile barrier (Morrow and Rhodes, 2001) would have greatly facilitated the establishment of a cross-formational fluid-flow system and the development of extensive convection cells, providing that there were spatial variations in relatively high basal heat flow. Fluid pathways within less permeable strata in the succession would have occurred along sets of vertical faults. If convection cells were able to incorporate subsurface, seawater-derived residual brines, as described in Morrow (1998) and earlier in Aulstead and Spencer (1985), extensive amounts of dolomite could result. The lack of clearly discernible regional trends and variations in the geochemistry and fluid inclusions of dolomites resulting from hydrothermal convection could, in part, locally reflect the depth to which convection cells circulated (Morrow, 1998), their temporal persistence, or, alternatively, variations in subsurface fluid-flow rates and the extent of water-rock interaction during convective circulation.

High heat flow and development of convection cells in the strata of the Western Canada Sedimentary Basin are also supported by Nelson et al.'s (2002) recent overview of western Canadian Mississippi Valley-type deposits. These authors concluded that earlier interpretations in previous studies, which suggested the involvement of fluid flow associated with the Devonian-Mississippian Antler Orogeny or the Cretaceous–Tertiary Laramide Orogeny, were inadequate to explain the distribution of base metal deposits and related, hosting dolomite in Western Canada. They suggested instead that various types of base metal deposits in the Cordillera and those at Pine Point were linked to regional plate-margin tectonics during the Late Devonian. During this time, thermal convection in an actively rifting back-arc setting led to volcanogenic and sedimentary exhalative metal deposits in the Cordillera, and Mississippi Valley deposits, such as Robb Lake and Pine Point, to the east in the Western Canada Sedimentary Basin.

CONCLUSIONS

The important conclusions of this study are the following:

1) The current work shows clearly that SD and most WTGD and MDGD mosaics have more or less identical cathodoluminescence characteristics, notably that inclusion-rich parts of crystals, usually cores, display blotchy luminescence, whereas the relatively inclusion-poor margins are dull or weak red luminescent, rarely nonluminescent, and sometimes show fine-scale compositional zoning. The correspondence of blotchy domains with the inclusion-rich portions of crystals suggests that at least some of this texture may result from pits from fluid inclusions transected by the surfaces of polished crystals. These blotchy domains could also be a compositional effect and the result of recrystallization.

2) Mosaics dominated by more fine-crystalline dolomite are typically more evenly dull luminescent overall. Dolomite crystals in partly dolomitized limestone with their nonluminescent cores and bright red rims are not present in the more thoroughly replacive mosaics, implying that these scattered crystals likely represent an earlier episode of dolomitization that had been thoroughly overprinted. Rare, brown-luminescent dedolomite indicates that localized dolomite alteration occurred either prior to or during precipitation of the late-stage, pore-filling calcite.

3) $\delta^{13}C$ and $\delta^{18}O$ values, $^{87}Sr/^{86}Sr$ and thermometric data from fluid inclusions are similar to those data obtained in Qing's (1991) study. However, our data do not show spatial trends that support the current paleohydrological model for the Middle Devonian Presqu'ile barrier, as described in Qing and Mountjoy (1994a). Rather, dolomitization of the Presqu'ile barrier may have resulted from the establishment of hydrothermal convection cells facilitated by the regional fracture framework, which allowed dolomitizing solutions to circulate. Circulation of convection cells to different depths, depending on local geological controls, could in part account for the absence of discernible $\delta^{18}O$, $^{87}Sr/^{86}Sr$ and fluid inclusion trends. Alternatively, a system of convection cells that have similar depths of circulation could also precipitate dolomite displaying nonlinear geographic trends of $\delta^{18}O$, $^{87}Sr/^{86}Sr$ and fluid inclusions because of temperature variations along flow paths and/or variations in the degree of recrystallization.

4) Fluid inclusion data indicate that samples can be differentiated on the basis of salinity but because SD and late-stage calcite recorded similar temperatures, fluid inclusion data may not have preserved the actual precipitation temperatures and temperature variation between SD and late-stage calcite. SD formed from high-salinity (20–35 wt.% NaCl equiv.) NaCl-$CaCl_2$ fluids and records no evidence of mixing with less saline fluids. Late-stage calcite formed from less saline (8–15 wt.% NaCl equiv.) NaCl fluids, suggesting minor mixing with less saline (meteoric) fluids.

ACKNOWLEDGMENTS

We thank the reviewers Keith Dewing and Ihsan Al-Aasm for their constructive comments. The Geological Survey of Canada through its Targeted Geoscience Initiative (TGI) project "Potential for carbonate-hosted Pb-Zn (MVT) deposits in northern Alberta and southern NWT" led by Peter Hannigan provided logistical support for this project. This research was partly supported by Coniglio's NSERC research grant while visiting the GSC (Calgary) on a recent sabbatical.

REFERENCES

Aulstead, K.L. and Spencer, R.J.
1985: Diagenesis of the Keg River Formation, northwestern Alberta: Fluid inclusion evidence; Bulletin of Canadian Petroleum Geology, v. 33, p. 167–183.

Bodnar, R.J.
1993: Revised equation and table for determining the freezing point depression of H_2O-NaCl solutions; Geochimica et Cosmochimica Acta, v. 57, p. 683–684.

Burke, W.H., Denison, R.E., Hetherington, E.A., Koepnick, R.B., Nelson, H.F., and Otto, J.B.
1982: Variation of seawater $^{87}Sr/^{86}Sr$ throughout Phanerozoic time; Geology, v. 10, p. 516–519.

Coniglio, M., Zheng, Q. and Carter, T.R.
2003: Dolomitization and recrystallization of middle Silurian reefs and platformal carbonates of the Guelph Formation, Michigan Basin, southwestern Ontario; Bulletin of Canadian Petroleum Geology, v. 51, p. 177–199.

Dorobek, S.L., Smith, T.M., and Whitsitt, P.M.
1993: Microfabrics and geochemistry of meteorically altered dolomite in Devonian and Mississippian carbonates, Montana and Idaho; *in* Carbonate Microfabrics, (ed.) R. Rezak and D.L. Lavoie; Springer-Verlag, New York, p. 205–225.

Fowler, M.G., Kirste, D.M., Goodarzi, F., and Macqueen, R.W.
1993: Optical and geochemical classification of Pine Point bitumens and evidence for their origin from two separate source rocks; Energy Sources, v. 15, p. 315–337.

Goldstein, R.H. and Reynolds, T.J.
1994: Systematics of fluid inclusions in diagenetic minerals; Society for Sedimentary Geology Short Course 31, 199 p.

Griffin, D.L.
1967: Devonian of northeastern British Columbia; *in* International Symposium on the Devonian System, Calgary, 1967, (ed.) D.H. Oswald; Volume 1, Alberta Society of Petroleum Geologists, p. 803–826.

Janicki, E.P.
2006: Distribution of Presqu'ile dolomite in the Great Slave Plain, Northwest Territories; *in* Potential for Carbonate-hosted Lead-zinc Mississippi Valley-type Mineralization in Northern Alberta and Southern Northwest Territories: Geoscience Contributions, Targeted Geoscience Initiative, (ed.) P.K. Hannigan; Geological Survey of Canada, Bulletin 591.

Krebs, W. and Macqueen, R.
1984: Sequence of diagenetic and mineralization events, Pine Point lead-zinc property, Northwest Territories, Canada; Bulletin of Canadian Petroleum Geology, v. 32, p. 434–464.

Leach, D.L. and Sangster, D.F.
1993: Mississippi Valley-type lead-zinc deposits; *in* Mineral Deposits Modeling, (ed.) R.V. Kirkham, W.D. Sinclair, R.I. Thorpe and J.M. Duke; Geological Association of Canada, Special Paper 40, p. 289–314.

Machel, H.G.
1997: Recrystallization versus neomorphism, and the concept of "significant recrystallization" in dolomite research; Sedimentary Geology, v. 113, p. 161–168.

MacLean, B.C.
2006: The sub-Phanerozoic basement surface under the Great Slave Plain of the Northwest Territories, and its influence on overlying strata; *in* Potential for Carbonate-hosted Lead-zinc Mississippi Valley-type Mineralization in Northern Alberta and Southern Northwest Territories: Geoscience Contributions, Targeted Geoscience Initiative, (ed.) P.K. Hannigan; Geological Survey of Canada, Bulletin 591.

Macqueen, R.W. and Powell, T.G.
1983: Organic geochemistry of the Pine Point lead-zinc ore field and region, Northwest Territories, Canada; Economic Geology, v. 78, p. 1–25.

Mazzullo, S.J.
1992: Geochemical and neomorphic alteration of dolomite: a review; Carbonates and Evaporites, v. 7, p. 21–37.

McNutt, R.H., Frape, S.K., Fritz, P., Jones, M.G., and MacDonald, I.M.
1990: The $^{87}Sr/^{86}Sr$ values of Canadian Shield brines and fracture minerals with applications to groundwater mixing, fracture history, and geochronology; Geochimica et Cosmochimica Acta, v. 54, p. 205–215.

Medford, G.A., Maxwell, R.J., and Armstrong, R.L.
1983: $^{87}Sr/^{86}Sr$ ratio measurements on sulfides, carbonates, and fluid inclusions from Pine Point, Northwest Territories, Canada: an $^{87}Sr/^{86}Sr$ ratio increase accompanying the mineralizing process; Economic Geology, v. 78, p. 1375–1378.

Morrow, D.W.
1998: Regional subsurface dolomitization: models and constraints; Geoscience Canada, v. 25, p. 57–70.

Morrow, D. and Rhodes, D.
2001: Pine Point stratigraphy and mineralization. Alexandra Falls Member reef complex and the Pine Point deposit (Part 2); Field trip guidebook, Canadian Society of Petroleum Geologists Annual Convention, June 18–22, 2001, 29 p.

Morrow, D.W., Zhao, M., and Stasiuk, L.D.
2002: The gas-bearing Devonian Presqu'ile dolomite of the Cordova embayment region of British Columbia, Canada: dolomitization and the stratigraphic template; American Association of Petroleum Geologists, Bulletin, v. 86, p. 1609–1638.

Morrow, D.W., MacLean, B.C., Miles, W.F., Tzeng, P., and Pană, D.
2006: Subsurface structures in southern Northwest Territories and northern Alberta: Implications for mineral and petroleum potential; *in* Potential for Carbonate-hosted Lead-zinc Mississippi Valley-type Mineralization in Northern Alberta and Southern Northwest Territories: Geoscience Contributions: Targeted Geoscience Initiative, (ed.) P.K. Hannigan; Geological Survey of Canada, Bulletin 591.

Mountjoy, E.W., Qing, H., and McNutt, R.H.
1992: Strontium isotopic composition of Devonian dolomites, Western Canada Sedimentary Basin: significance of sources of dolomitizing fluids; Applied Geochemistry, v. 7, p. 59–75.

Nelson, J., Paradis, S., Christensen, J., and Gabites, J.
2002: Canadian Cordilleran Mississippi Valley-type deposits: a case for Devonian-Mississippian back-arc hydrothermal origin; Economic Geology, v. 97, p. 1013–1036.

Nielsen, P., Swennen, R., and Keppens, E.
1994: Multiple-step recrystallization within massive ancient dolomite units: an example from the Dinantian of Belgium; Sedimentology, v. 41, p. 567–584.

Popp, B.N., Anderson, T.F., and Sandberg, P.A.
1986: Textural, elemental and isotopic variations among constituents in Middle Devonian limestones, North America; Journal of Sedimentary Petrology, v. 56, p. 715–727.

Qing, H.
1991: Diagenesis of Middle Devonian Presqu'ile dolomite, Pine Point, NWT and adjacent subsurface; Ph.D. thesis, McGill University, Montreal, Quebec, 292 p.

Qing, H. (cont.)
1998a: Petrography and geochemistry of early-stage, fine- and medium-crystalline dolomites in the Middle Devonian Presqu'ile barrier at Pine Point, Canada; Sedimentology, v. 45, p. 433–446.
1998b: Geochemical constraints on the origin and timing of palaeofluid flow in the Presqu'ile barrier reef, Western Canada Sedimentary Basin; *in* Dating and Duration of Fluid Flow and Fluid-rock Interaction, (ed.) J. Parnell; Geological Society, London, Special Publications 144, p. 173–187.

Qing, H. and Mountjoy, E.W.
1989: Multistage dolomitization in Rainbow buildups, Middle Devonian Keg River Formation, Alberta, Canada; Journal of Sedimentary Petrology, v. 59, p. 114–126.
1994a: Formation of coarsely-crystalline, hydrothermal dolomite reservoirs in the Presqu'ile barrier, Western Canada Sedimentary Basin; American Association of Petroleum Geologists, Bulletin, v. 78, p. 55–77.
1994b: Origin of dissolution vugs, caverns, and breccias in the Middle Devonian Presqu'ile barrier, host of Pine Point Mississippi Valley-Type deposits; Economic Geology, v. 89, p. 858–876.
1994c: Rare earth element geochemistry of dolomites in the Middle Devonian Presqu'ile barrier, Western Canada Sedimentary Basin: implications for fluid-rock ratios during dolomitization; Sedimentology, v. 41, p. 787–804.

Rhodes, D., Lantos, E.A., Lantos, J.A., Webb, R.J., and Owens, D.C.
1984: Pine Point orebodies and their relationship to the stratigraphy, structure, dolomitization, and karstification of the Middle Devonian barrier complex; Economic Geology, v. 79, p. 991–1055.

Sibley, D.F. and Gregg, J.M.
1987: Classification of dolomite rock textures; Journal of Sedimentary Petrology, v. 57, p. 967–975.

Skall, H.
1975: The paleoenvironment of the Pine Point lead-zinc district; Economic Geology, v. 70, p. 22–47.

Stasiuk, L.D. and Snowdon, L.R.
1997: Fluorescence micro-spectrometry of synthetic and natural hydrocarbon fluid inclusions: crude oil chemistry, density and application to petroleum migration; Organic Geochemistry, v. 12, p. 229–241.